Universidade de Aveiro Departamento de Química
2017

Bruno Miguel Martins Zêzere

Difusividades de compostos bioativos em misturas supercríticas e solventes expandidos

Diffusivities of bioactive compounds in supercritical mixtures and expanded solvents

Universidade de Aveiro Departamento de Química
2017

Bruno Miguel Martins Zêzere

Difusividades de compostos bioativos em misturas supercríticas e solventes expandidos

Diffusivities of bioactive compounds in supercritical mixtures and expanded solvents

Dissertação apresentada à Universidade de Aveiro para cumprimento dos requisitos necessários à obtenção do grau de Mestre em Engenharia Química, realizada sob a orientação científica do Doutor Carlos Manuel Santos da Silva, Professor auxiliar do Departamento de Química da Universidade de Aveiro.

Dedico esta dissertação aos meus pais e irmã.

o júri

presidente

Professor Doutor Francisco Avelino da Silva Freitas
Professor auxiliar do Departamento de Química da Universidade de Aveiro

Doutor António Augusto Areosa Martins
Investigador de Pós-doutoramento do Laboratório de Engenharia de Processos, Ambiente, Biotecnologia e Energia, Faculdade de Engenharia da Universidade do Porto

Professor Doutor Carlos Manuel Santos da Silva
Professor auxiliar do Departamento de Química da Universidade de Aveiro

agradecimentos

Agradeço a todo o grupo EgiChem pelo apoio e amizade ao longo destes últimos meses. Um obrigado em especial ao meu orientador, Doutor Carlos Manuel Silva, por todo o apoio, amizade e motivação. Um obrigado também à Doutora Ana Magalhães, por toda a sua ajuda nos primeiros meses de realização desta tese, e à Doutora Inês Portugal, pela atenção que dedicou ao meu trabalho e à revisão da dissertação.

Agradeço ainda a todos aqueles que me acompanharam ao longo deste percurso e que me ajudaram a crescer e a ser quem sou hoje.

Finalmente gostaria de deixar um obrigado muito especial aos pais, irmã e namorada que ao longo destes cinco anos sempre me apoiaram e motivaram, sem eles certamente não teria chegado ao fim desta etapa.

palavras-chave

Coeficiente de Difusão, Eucaliptol, Dióxido de carbono supercrítico, Cossolvente, Modelação

resumo

Nas últimas décadas, os fluidos supercríticos têm ganho maior destaque no âmbito dos paradigmas de biorrefinaria e sustentabilidade de processos químicos, surgindo como alternativa *verde* a muitos solventes orgânicos. Em particular, sendo o dióxido de carbono supercrítico (SC-CO_2) o solvente preferido, são necessários valores experimentais e modelos preditivos de difusividades de solutos tanto em SC-CO_2 puro como modificado com cossolvente. Esta tese surge como resposta à falta de dados e modelos nesta área, tendo como principal objetivo a medição e posterior modelação dos coeficientes de difusão de eucaliptol em SC-CO_2 modificado com 8 % (m/m) de etanol e ainda etanol líquido puro.

Recorrendo ao método cromatográfico de abertura de pico (CPB), procedeu-se à medição de difusividades do eucaliptol a diluição infinita (D_{12}), numa gama de temperaturas entre 303.15 K e 333.15 K. Para a mistura SC-CO_2 com etanol, a pressões de 150 a 275 bar, obtiveram-se valores compreendidos entre 0.547×10^{-4} a 1.042×10^{-4} cm^2 s^{-1}. Já em etanol puro, variando a pressão entre 1 e 100 bar, obtiveram-se difusividades entre 0.912×10^{-5} e 1.578×10^{-5} cm^2 s^{-1}. Os resultados de D_{12} foram analisados em função da temperatura, pressão, densidade e em coordenadas de Stokes-Einstein.

Testou-se também uma série de modelos baseados nas teorias hidrodinâmica e de volume livre, bem como equações empíricas. Os valores calculados e experimentais foram comparados com base no desvio relativo absoluto médio (AARD). Para ambos os sistemas, destacam-se o modelo de dois parâmetros de Dymond-Hildebrand-Batschinski (DHB), o modelo Tracer Liu-Silva-Macedo com um parâmetro ($TLSM_d$), um modelo modificado Stokes-Einstein-1, e as relações empíricas de Magalhães *et al.* (AARD entre 1.2 e 7.0 %). Em relação ao sistema ternário (eucaliptol na mistura SC-CO_2 com etanol) os modelos de Wilke-Chang, Lai-Tan e Vaz *et al.* (AARD de 8.00, 8.36 e 1.29 %, respetivamente) foram os melhores. Quanto ao sistema binário (eucaliptol em etanol líquido) destaca-se ainda o modelo de Tracer Liu-Silva-Macedo (TLSM) (AARD de 6.75 %). Sugerem-se ainda correções a dois modelos, nomeadamente, à extensão do modelo de Liu-Silva-Macedo para intradifusividades em mixturas Lennard-Jones multicomponente, usando as regras de mistura propostas por Merzliak e Pfenning (LSM-MP) para o sistema ternário, e ao modelo DHB para o sistema binário, tendo-se obtido AARDs de 1.55 % e 3.70 %, respetivamente.

Finalmente, procedeu-se à modelação de uma base de dados contendo 1453 pontos experimentais de difusividades correspondentes a 132 sistemas ternários distintos. Esta modelação foi realizada utilizando o modelo LSM-MP, ao qual foi proposta uma correção com base na divisão dos dados em 2 grupos: sistemas líquidos e supercríticos (AARDs de 9.39 % e 9.11 %, respectivamente).

keywords

Diffusion coefficient, Eucalyptol, Supercritical Carbon Dioxide, Cosolvent, Modelling

abstract

Supercritical fluids have gained great importance within the concepts of biorefinery and sustainability of chemical processes. They are considered a “greener” alternatives to a vast group of conventional organic solvents with supercritical carbon dioxide (SC-CO_2) being the most preferred. Currently, experimental data and predictive models for diffusivity in SC-CO_2 systems are scarce especially regarding SC-CO_2 systems modified with a cosolvent. The main objective of this thesis was the experimental determination and modelling of tracer diffusion coefficients (D_{12}) of eucalyptol in SC-CO_2 expanded with 8 wt.% ethanol (ternary system) and in pure ethanol (binary system). Furthermore improve the D_{12} modelling in multicomponent mixtures.

Eucalyptol diffusivities were measured by the chromatographic peak broadening technique (CPB) in the temperature range 303.15 to 333.15 K. For the ternary system the values ranged from 0.547×10^{-4} to 1.042×10^{-4} $cm^2\cdot s^{-1}$ for pressures between 150–275 bar. For the binary system the values ranged from 0.912×10^{-5} to 1.578×10^{-5} $cm^2\cdot s^{-1}$ for pressures between 1-100 bar. The dependency of D_{12} in terms of temperature, pressure, solvent density, and Strokes-Einstein coordinates were also examined.

A series of models based on hydrodynamic and free volume theory and on empirical correlations were tested and compared using the average absolute relative error (AARD) for calculated and experimental values. For both systems, the best results were obtained with the two parameter Dymon-Hildebrand-Batschinski (DHB) model, with the one parameter Tracer Liu-Silva-Macedo ($TLSM_d$) model, with the modified Stokes-Einstein-1 model, and with the Magalhães *et al* correlations (AARD between 1.2 and 7.0 %). For the ternary system the Wilke-Chang, Lai-Tan, and Vaz *et al.* models can also be highlighted (achieving AARD of 8.00, 8.36 and 1.29 % respectively). For the binary system the TLSM model achieves an error of 6.75 %. In addition, two corrections are presented to improve model fitting, namely for the extension of Liu-Silva-Macedo model to multicomponent LJ intradiffusivities using mixing rules of Merzliak and Pfenning (LSM-MP) applied to the ternary system and for the DHB model applied to the binary system (AARD of 1.55 % and 3.70 %, respectively).

Finally a database containing 132 ternary systems with a total of 1453 experimental diffusivity values was utilized for modeling D_{12} values, on the basis of the LSM-MP model. The AARD results obtained by splitting the database into two groups, namely liquid and supercritical systems, were 9.39 and 9.11 % respectively.

Contents

Figure index

Table Index

Nomenclature

Absmax	Maximum absorbance	(Dimensionless)
Apeak	Peak area	(Dimensionless)
b_{VD}	Optimized parameter from the DHB model correction	(mol m^{-3})
B_{DHB}	Interaction solute-solvent parameter in the DHB model	(cm^{-1}·mol·s^{-1} $K^{-1/2}$)
C_2	Tracer's concentration	(mol m^{-3})
C^{app} (z,t)	Calculated average radial concentration of the solute	(mol m^{-3})
C^{exp} (z,t)	Solute concentration at exit column	(mol m^{-3})
C_t	Total concentration	(mol m^{-3})
D	Dispersion coefficient	(m^2 s^{-1})
D_{12}	Tracer diffusion coefficient of solute 2 through solvent 1	(m^2 s^{-1})
D_{12}^b	Background term of the Vaz *et al.* model	(m^2 s^{-1})
D_{12}^s	Singular term of the Vaz *et al.* model	(m^2 s^{-1})
De	Dean number, De=Re/$\sqrt{\xi}$	(Dimensionless)
H	Height of theoretical plate	(m)
$J_{1,z}$	Total unidimensional flux	(m^2 mol s^{-1})
k	Retention factor	(Dimensionless)
$k_{12,d}$	Binary interaction constant	(Dimensionless)
k_B	Boltzmann constant	(1.380658×10^{-23} J K^{-1})
K_r	Refractive index	(Dimensionless)
L	Length of the column	(m)
m	Total mass of solute injected	(mol)
m_{VD}	Optimized parameter from the DHB model correction	(m^3 mol^{-1} K^{-1})
m_i	Particle mass	(g)
M	Molecular weight	(g mol^{-1})
M_{12}	Reduced molar mass	(Dimensionless)
N_{av}	Avogadro's number	($6.022\times10^{23}$$mol^{-1}$)
P	Pressure	(kg m^{-1} m^2)
P_c	Critical pressure	(kg m^{-1} m^2)
r	radial coordinate	(m)

R	Inner column radius	(m)
R_c	Tube coil radius	(m)
Re	Reynolds number (Re= u ρ R /μ)	(Dimensionless)
R_g	Universal gas constant	(8.3144 J mol^{-1} K^{-1})
S	Zeroth moment	(mol dm^{-3} s)
Sc	Schmidt number Sc= $\mu_1/\rho_1 D_{12}$	(Dimensionless)
S_{10}	Asymmetric factor	(Dimensionless)
t	Time	(s)
t_i	Time at 10% peak height in the fitting method	(s)
t_r	Retention time	(s)
$\bar{t}$	Average retention time	(s)
T_i^*	Reduced Temperature using LJ energy component i	(Dimensionless)
T	Absolute temperature	(K)
T_{bp}	Normal boiling temperature of the component I	(K)
T_c	Critical temperature	(K)
$\bar{u}$	Average linear velocity	(m s^{-1})
$\bar{u}_{opt}$	Optimum average linear velocity	(m s^{-1})
V_c	Critical molar volume	(m^3 mol^{-1})
V_D	Maximum packaging volume of the solvent in the DHB model	(m^3 mol^{-1})
V_m	Molar volume	(m^3 mol^{-1})
$V_{TC,bp,i}$	Molar volume of the component *i* at its normal boiling point estimated by the method of Tyn and Calus	(m^3 mol^{-1})
$W_{0.607}$	Peak half-width measured at 60.7% of total peak height	(s)
x_i	Molar composition of the component *i*	(Dimensionless)
z	Axial coordinate	(m)
z'	Axial coordinate corrected by the fluid displacement	(m)

Greek letters

Γ_{12}^{∞}	Thermodynamic factor at infinite dilution	(Dimensionless)
$\delta(z)$	Dirac's function	(Dimensionless)
ε	Root mean square deviation	(Dimensionless)

$\varepsilon_{LJ,i}$	LJ parameter of componente i = 1, 2 or mixture i = 12	(K)
ζ	Curvature ratio	(Dimensionless)
λ	Wavelength	(nm)
θ	Merzliak and Pfenning model parameters (1 to 5)	(Dimensionless)
μ_1	Solvent viscosity	(kg m^{-1} s^{-1})
ρ_1	Solvent density	(kg m^{-3})
$\rho_{n,1}$	Solvent numerical density	(m^{-3})
σ_i	Molecular diameter of component *i*	(m)
$\sigma_{LJ,i}$	Lennard-Jones diameter of component *i*	(m)
ϕ	Solvent association factor in the Wilke-Chang equation	(Dimensionless)
ω	Acentric factor	(Dimensionless)

Subscripts

1	Solvent
2	Solute
12	Binary
bp	Property evaluated at normal boiling point
c	critical property
eff	Effective
i	Component i
j	Component j
LJ	Lennard-Jones
mix	Mixture
TC	Tyn-Calus

Superscripts

I	Input
II	Output
∞	Infinite dilution
*	Reduced quantity
app	Aproximated mean
calc	Calculated

exp	Experimental

Abbreviations

AARD	Average absolute relative deviation
BPR	Back pressure regulator
CPB	Chromatographic Peak Broadening method
DHB	Dymond-Hildebrand-Batchinski
LJ	Lennard-Jones
LSM-MP	Liu-Silva-Macedo model for multicomponent intradiffusivities using mixing rules of Merzliak and Pfenning
LSM-MP-θ_1	Improved LSM-MP model (LSM parameters and re-optimized θ_1)
mSE_1	modified Stokes-Einstein-1
NDP	Number of data points
SC–CO_2	Supercritical carbon dioxide
SFC	Supercritical fluid
TLSM	Tracer diffusion coefficient model of Liu, Silva and Macedo
UV	Ultraviolet

1. Introduction

Increasing attention has been given over past decades to the biorefinery and sustainability concept leading to the substitution of organic solvent by green alternatives, like supercritical fluids (SCF) [1]. These fluids offer a clean and environmentally friendly alternative to some of the organic solvents used in extraction, purification and reactional processes [2–6]. SCFs are characterized by having densities similar to liquids, values of viscosity close to gas and diffusivities between those of gas and liquids. These characteristics combined with their great capacity of changing their solvent power with small variations of temperature and/or pressure, in the vicinity of the critical point, give them a tremendous potential for being used as solvents in the previously mentioned processes. Presently the SCF have found several advances in various distinct areas such as food and pharmaceutical industry, environmental and material applications and also in chromatography as mobile phase [5–7]. Through the last one it is possible to analyze and to separate thermally instable and low volatile compounds, it is also possible to determine physico-chemical properties of fluid systems like diffusivities [8] . Some more practical applications of the SCF are of example the triterpenoids extraction and purification [9], extraction of vegetable matrices [10], spent coffee grounds [11], coffee and tea decaffeination [12].

Carbon dioxide is the most preferable solvent to be used as SCF due to its characteristics, it is nontoxic, nonflammable, cheap and has near-ambient critical temperature, 304.1 K, and a low critical pressure, 73,8 bar [12]. It is globally a nonpolar molecule but possesses a quadrupole moment. Hence, nonpolar and weakly polar molecules easily dissolve in supercritical CO_2 (SC-CO_2), in contrast polar and heavy molecules have very low solubilities. The polarity of the SC-CO_2 can be improved by adding an entrainer such as acetone, methanol, or the one used in this study ethanol [8,12]. This resulted in an increasing interest upon SC-CO_2 to substitute organic solvents, leading to a need of knowing its transport properties in order to be possible to carry out accurate process simulations and equipment design [8,13]. Some of the most important properties in question are the viscosity, thermal conductivity and finally the one studied in this work, the diffusion coefficient of a solute 2 though solvent 1 (D_{12}).

Diffusion is one of the two main existing mass transfer mechanisms being the other one by convection. The latest is described as the macroscopic motion of molecules while the first is defined as the random and spontaneous microscopic movement that results from the thermal movement of the molecules [14].

The molecular motion by diffusion is described by the Fick's law, which has as base three observations quantified by Fick in 1855 [14]:

- Mass transfer phenomenon occurs due to a concentration gradient, which mean, in the case of a binary mixture, the molecular species diffuses to the lower concentration medium;
- The mass transfer rate is proportional to the area normal to the mass transfer direction. Thus, it can be expressed as a flux;
- Net transfer stops once uniformity is reached.

Fick suggested an analogy to the first law of heat conduction, thus the Fick law was defined as Eq.1. This equation shows proportionality between a flux and a gradient where $J_{2,z}$ defines the total unidimensional flux per area unit, C_t represents the total concentration, x_2 the fraction of species 2 fraction, z the distance and D_{12} the diffusion coefficient of component 2 thought 1 [15].

$$J_{2,z} = -D_{12} C_t \frac{dx_2}{dz} \quad \text{(Eq.1)}$$

It is important to mention that accurate the driving force of Fick's law is the gradient of chemical potential; the concentration gradient is frequently used as an approximation [16].

Currently it is verified a lack of D_{12} data specially supercritical mixtures (eg: SC-CO_2 modified with ethanol) [17], or in the case of known systems, the existence of accurate models for D_{12} prediction [18]. This work comes in response to this lack of data having been performed D_{12} measurements of eucalyptol in SC-CO_2 modified with ethanol and in liquid ethanol. Then it was performed to the data modelling using several models ranging from classical and more recent models based on hydrodynamic and free volume theories.

The solute in study, eucalyptol, is a monocyclic monoterpene, also known as 1,8-cineol, with molecular form $C_{10}H_{18}O$. This compound is liquid under atmospheric conditions; and presents odor but no color. The compound can be found in natural oils, being viable from *Eucalyptus* essential oils since it is present in high concentrations (up to 90 %). Isolation from the other terpenes can be accomplished by various processes including conventional solvent extraction, cold treatment with a strong acid (e.g. H_2SO_4) [19], and a two-step

distillation process in the presence of phenols [20]. In the past eucalyptol was used as antiseptic and expectorant, currently it founds applications in the pharmaceutical industry, due to his bioactive properties, being presented in medicinal drugs used as a remedy for symptoms of the common cold and other respiratory infections [21]. It possesses substantial antibacterial activity [22], it is used as perfume and fragrance [19], and presents potential to replace certain petroleum-based solvents used as industrial degreasers [23].

The present thesis is divided into six chapters. In Chapter 2 "Fundaments of D_{12} experimental determination", it will be discussed the experimental fundaments for D_{12} measurement; In Chapter 3 "Tracer diffusion coefficients models" the models used for modelling the data obtained are presented and discussed; In Chapter 4 "Experimental section" a description of the equipment, experimental procedure and conditions, chemicals and the correlations used to calculate density and viscosity of the solvent are presented. In Chapter 5 it is discussed the data measured and calculated regarding both ternary (eucalyptol/SC-CO_2/ethanol) and binary (eucalyptol/ethanol) systems, together with modeling results of a compiled D_{12} ternary systems database. Finally in Chapter 6 the main conclusions of this work are compiled as well as future work suggestions.

The current dissertation produced an international publication, and a second manuscript is under preparation.

2. Fundaments of D_{12} experimental determination

The experimental determination of the binary diffusion coefficient, D_{12}, of organic compounds in supercritical fluids and liquid solvents can be done by five different methods: solid dissolution technique (SD), photon correlation spectroscopy (PCS), nuclear magnetic resonance (NMR), radioactive tracer response (RTR) and the one used in this study, the chromatographic peak broadening technique (CPB) [24].

2.1. Chromatographic peak broadening technique (CPB)

The CPB technique is a chromatographic method based on the work of Taylor [25–27] later continued by Aris [28]. Taylor showed that when a pulse of solute is injected in a laminar solvent stream thought a capillary strait tube of circular cross section, the pulse will broaden due to the combined action of convection, along the axis of the tube, and molecular diffusion in radial direction [24]. Although the original work conducted by Taylor and Aris was uniquely devoted to describe a solute pulse dispersion in straight tubes under laminar flow, only then the method was specifically applied for the measurement of diffusion coefficients of solutes in gases [29], dense gases [30], liquid [31] and later in SCF [32]. Based on this technique it is possible to obtain results in a short time period, however the D_{12} values obtained correspond to coefficients at infinite dilution, due to the small quantity of solute utilized (e.g. 0.2 – 1.0 μL [33,34]), being impossible to determine the relation between D_{12} and the solute concentration [24]. The typical response resulting from this method is represented in Figure 1 [35]. As can be observed when a pulse of a diluted solute in introduced in an organic solvent stream, the peak of both compounds will come out of the column together if no adsorbent phase existing in the column. This limits the method to solutes not diluted in organic solvents, since the peak obtained would be of the mixture of solute and solvent.

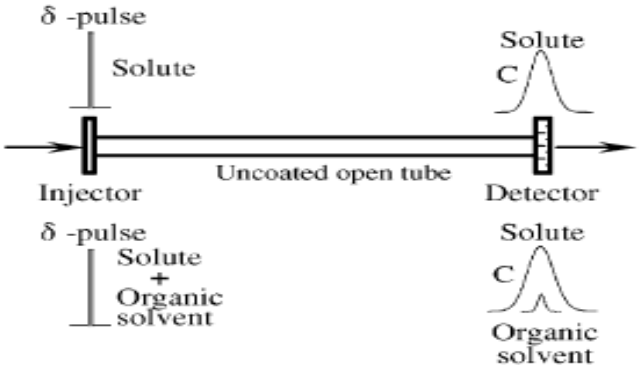

Figure 1 – Typical response of Taylor-Aris (CPB) method to an impulse input signal [35].

If the pulse is introduced in a laminar flow solvent stream in a cylindrical column, and the assumption that the physical properties are constant during each measurement can be made, the tracer concentration, C_2, can be expressed as function of time, t, and the axial and radial coordinates z and r. The concentration profile is given by [36]:

$$\frac{\partial C_2}{\partial t} = D_{12}\left[\frac{1}{r}\frac{\partial}{\partial \mathrm{r}}\left(r\frac{\partial C_2}{\partial r}\right) + \frac{1}{r^2}\frac{\partial^2 C_2}{\partial z^2}\right] - 2\bar{u}\left(1 - \frac{r^2}{R^2}\right)\frac{\partial C_2}{\partial z} \qquad \text{(Eq.2)}$$

where R is the column inner radius and $\bar{u}$ the mean velocity of the solvent stream.

The time required in order to observe concentration effects due to axial convection is very long compared to the effect of radial variations. If the condition given by Eq.3 is respected, the axial dispersion component, $\frac{1}{r^2}\frac{\partial^2 C_2}{\partial z^2}$, can be neglected in comparison to radial dispersion component, $\frac{1}{r}\frac{\partial}{\partial r}\left(r\frac{\partial C_2}{\partial r}\right)$ [25].

$$\frac{L}{\bar{u}} \gg \frac{R^2}{3\times 8^2 D_{12}} \qquad \text{(Eq.3)}$$

where L is the column length.

Taking this approximation into account, Eq.2 can be written as Eq.4:

$$\frac{\partial C_2}{\partial t} = D_{12}\left[\frac{1}{r}\frac{\partial}{\partial r}\left(r\frac{\partial C_2}{\partial r}\right)\right] - 2\bar{u}\left(1 - \frac{r^2}{R^2}\right)\frac{\partial C_2}{\partial z} \qquad \text{(Eq.4)}$$

The initial and boundary conditions imposed to Eq.4 are:

$t = 0$, $$C_2 = \frac{m}{\pi R^2}\delta(z) \qquad \text{(Eq.5)}$$

$t \geq 0$, $$\frac{\partial C_2}{\partial r} = 0 \text{ for } r = 0 \text{ and } r = R \qquad \text{(Eq.6)}$$

$$C_2 = 0 \text{ for } z = \pm\infty \qquad \text{(Eq.7)}$$

where m it is the quantity of injected solute and $\delta(z)$ the Dirac's function.

In most experiments, average concentration over the cross-sectional area of tubing, C^{app}, is measured by the UV detector calculated by:

$$C^{app} = \frac{2}{R^2}\int_0^R C_2\,(r,z,t)\,\mathrm{d}r \qquad \text{(Eq.8)}$$

Combining Eq.4 to Eq.7 it is obtained:

$$\frac{\partial C^{app}}{\partial t} = D\frac{\partial^2 C^{app}}{\partial z^2} - \bar{u}\frac{\partial C^{app}}{\partial z} \qquad \text{(Eq.9)}$$

where C^{app} it is the mean concentration, D the dispersion coefficient described by Taylor and given by Eq.10 which combines both effects of radial and axial dispersion [28].

$$D = D_{12} + \frac{R^2\bar{u}^2}{48D_{12}} \qquad \text{(Eq.10)}$$

The initial and boundary conditions of Eq.9 are:

$$C^{app} = \frac{m}{\pi R^2}\delta(z) \text{ for } t = 0 \qquad \text{(Eq.11)}$$

$$C^{app} = 0 \text{ for } z = \pm\infty \qquad \text{(Eq.12)}$$

By combining Eqs.9-12 it is obtained the solute average concentration, C^{app}, of the solute inside the column:

$$C^{app} = \frac{m}{\pi R^2}\frac{1}{\sqrt{4\pi Dt}}\exp\left[-\frac{(z-\bar{u}t)^2}{4Dt}\right] \qquad \text{(Eq.13)}$$

The peak concentration profile can also be described mathematically in terms of the variance of the peak in unity of square meter, σ^2, by Eq.14.

$$\sigma^2 = \frac{2DL}{\bar{u}} = \frac{2D_{12}L}{\bar{u}} + \frac{R^2\bar{u}L}{24D_{12}} = HL \qquad \text{(Eq.14)}$$

which in terms of the theoretical plate height, H, can be written as:

$$H = \frac{\sigma^2}{L} \qquad \text{(Eq.15)}$$

Equations 14 and 15 were derived for straight tubes, however to be possible to measure diffusivities accurately the tube must be at constant temperature. Since the tubes may have considerable length they must be coiled in order to be placed in a constant temperature bath or oven. This configuration has two main implications, as reported by Nunge *et al.* [37]: first, the velocity profile is elongated, leading to a greater dispersion of the peak creating a situation where lower apparent diffusivity values are obtained; second, it is present a centrifugal effect that sets up secondary flow perpendicular to the flow direction leading to an incensement of the mixing results in narrower peaks that generates higher apparent diffusivity values [38]. Once the fluid is thrown out, since mass accumulation cannot occur there is a formation of a secondary-flow in the opposite direction that

compensates the outward flow, causing a circular movement from the interior to the exterior of the column (Figure 2) [39].

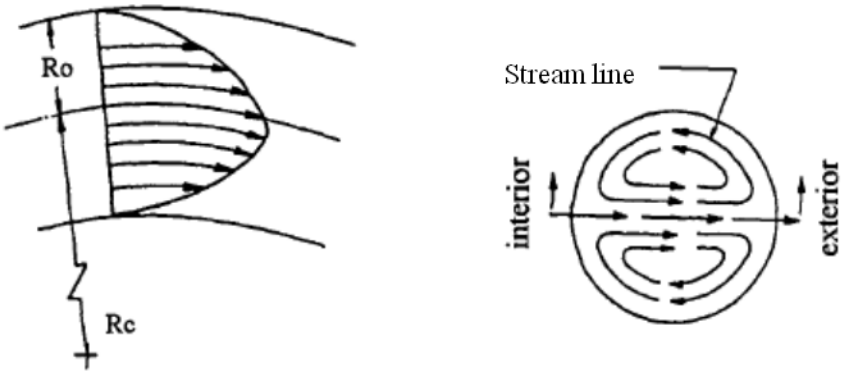

Figure 2 – Schematic representation of laminar flow velocity profile in a coiled tube [39].

The previous description leads to a deviation to the Taylor-Aris assumptions that can be expressed as function of the Reynolds (Re, Eq.16) and Schmidt (Sc, Eq.17) numbers, and by the geometric factor ζ. The curvature of the coil is characterized by ζ calculated by the ratio between the tube coil radius, R_C, and the inner column radius, R. Under certain conditions Re and ζ are not independent, in fact the relation between centrifugal and inertia forces is described by the Dean number (De), (Eq.18) [38,39].

$$\mathrm{Re} = \frac{\bar{u}\,\rho_1\,R}{\mu_1} \qquad \text{(Eq.16)}$$

$$\mathrm{Sc} = \frac{\mu_1}{\rho_1\,D_{12}} \qquad \text{(Eq.17)}$$

$$\mathrm{De} = \mathrm{Re}\zeta^{-0.5} \qquad \text{(Eq.18)}$$

These dimensionless numbers can also describe the peak's behavior. The peak broadening effect is due to a proportional term to $\mathrm{Re}^2\mathrm{Sc}\zeta^{-2}$, which dominates at lower Re if $\zeta < 10$. On the other hand the narrowed peak effect is proportional to $\left(\mathrm{De}^2\mathrm{Sc}\right)^2$ which is dominant at higher Re values [37,38].

In order to neglect temperature and pressure perturbations, then may occur outside the oven, van der Laan [40] defined that the following condition must be respected [33]:

$$\frac{\bar{u}L}{D} > 1000 \qquad \text{(Eq.19)}$$

The secondary flow effects in the column can be neglected if the flowing condition is met:

$$\mathrm{DeSc}^{0.5} < 10 \qquad \text{(Eq.20)}$$

This criterion was proposed by Moulijin *et al.*[41], Alizadeth *et al.*[42] and Springston and Novotny [43]: to guaranty an error lower than 1 %, Funazukuri [35,44] recommends that $\mathrm{DeSc}^{0.5}$ should be lower than 8.

Finally in order to the solute concentration profile approximate a gaussian form, according to Levenspiel and Smith [45], the following condition should be met:

$$\frac{D}{\bar{u}L} < 0.01 \qquad \text{(Eq.21)}$$

If the previous mentioned conditions are respected, the D_{12} value can be determined by [33]:

$$D_{12} = \frac{\bar{u}}{4}\left[H \pm \left(H^2 - \frac{R^2}{3}\right)^{0.5}\right] \qquad \text{(Eq.22)}$$

The theoretical plate height, H, can be calculated by different methods. One of the most simple and precise methods consists in measuring the half width of the peak at a 60.7 %, height, $W_{0.607}$, and then use [24]:

$$H = \frac{LW_{0,607}^2}{{t_r}^2} = \frac{\bar{u}^2 W_{0,607}^2}{L} \qquad \text{(Eq.23)}$$

where t_r is the retention time and $W_{0.607}$ is expressed in time units.

It should be noted that Eq.22 is a quadratic equation meaning that two possible solutions may appear. Giddings and Seager [46] have shown that the best way to determine them is by calculating H using various values of speed and an arbitrary value of D_{12} in Eq.14 and 15. Then by calculating D_{12} using Eq.22 two solutions are obtained. For velocities up to the optimum velocity, u_{opt}, the positive root should be taken, for values higher than u_{opt}, the negative root is taken. The optimum velocity, u_{opt}, which minimizes the value of H, is calculated using Eq.24. When working with liquids and dense fluids, the negative root should be chosen since the optimum velocity is very low and easily overcome by the solvent [24].

$$u_{opt} = \sqrt{48}\frac{D_{12}}{R} \qquad \text{(Eq.24)}$$

The chromatographic peak broadening (CPB) method it is a very precise and fast method to determine diffusion coefficients. Unfortunately, this method suffers from constrains, most of them discussed previously. The method is not appropriate for measuring diffusion coefficients in the vicinity of the critical point due to the reduced solvent power of the supercritical fluid. The mixture solute/SC-CO_2 does not attain the

supercritical state in most of axial positions of the column leading to abnormal peaks when large amount of solute is injected [8,35]. The method is also very sensible to pressure drops, initial solute dispersion and secondary flow discussed previously. Finally the method also neglects adsorption of the solute onto column wall [47], but if adsorption is present asymmetry and tailing should be notice in the outlet chromatogram [24,48]. Special attention should be given to the columns material in order to neglect solute adsorption. Diffusion coefficients polar compounds or high molecular weight compounds cannot be determined using this method since peak tailing caused by adsorption leads to a significant degree of error [8,35].

To calculate the D_{12} values from the response curves obtained, three methods can be applied: the previously described (Eqs.22-23) graphical method. [26,49], the moments method, and the fitting method.

The moments method consists in determining D_{12} thought the zeroth, first and second moments of the peak signal.

If $D_{12}\bar{t}/R^2 > 10$ and combining Eq.10 and 25 (Eq.25 describes the variance of the error function) Eq.26 is obtained, having maximum error of ± 1 % associated.

$$\sigma^2 = \frac{2D\bar{t}}{\bar{u}^2} \quad \text{(Eq.25)}$$

$$D_{12} = \frac{R^2\bar{t}}{24\sigma^2} \quad \text{(Eq.26)}$$

where $\bar{t}$ is the average retention time and σ^2 is the variance. Both can be obtained by the zeroth, first and second moments [49]:

$$S = \int_0^\infty C(t)\ \mathrm{d}t \quad \text{(Eq.27)}$$

$$\bar{t} = \frac{1}{S}\int_0^\infty C(t)\ \mathrm{d}t \quad \text{(Eq.28)}$$

$$\sigma^2 = \frac{1}{S}\int_0^\infty \left(t - \bar{t}\right)^2 C(t)\ \mathrm{d}t \quad \text{(Eq.29)}$$

By using the fitting method $\bar{t}$ e σ^2 are calculated by nonlinear fitting of the peak, minimizing the root mean square error, ε, given by Eq.30 [50].

$$\varepsilon = \left(\frac{\int_{t1}^{t2}\left(C^{\exp}(t) - (C^{\mathrm{app}}(L,t)\right)^2 \mathrm{d}t}{\int_{t1}^{t2}\left(C^{\exp}(t)\right)^2 \mathrm{d}t}\right)^{1/2} \quad \text{(Eq.30)}$$

where $C^{\exp}$ is the concentration experimentally determined. The variables t_1 and t_2 are time values selected at 10 % of peak height, being $t_1 < t_2$ [17,36]. Taking into account the values of ε, the fitting can be considered good if the value of ε is less than 1 %, the fitting

is acceptable if the value is situated between 1 % and 3 %, and for values higher than 3 % it is rejected [35,50]. Another parameter used to quantify the chromatographic peak is the asymmetry factor; if this value is higher than 1.1-1.3, the peak should be rejected [17,24,51].

Between the last two method presented the fitting method is considered more precise than the moment method [35]. According to Wako and Kaguei [52] the moment method overestimates the errors related to the frontal and tailing portions of the response curve, and such limitations can be overcome by the fitting method [36].

2.2. Chromatographic impulse response technique (CIR)

The chromatographic impulse response (CIR) technique is also utilized to measure diffusion coefficients at infinite dilution of gases, liquids and supercritical fluids. The greatest difference from the previous method (CPB) is the usage of a column with a polymeric coating, which causes the chromatographic separation of the solute from the solvent due to different retention times, if a solution is inject instead of a pulse of a pure liquid solute. This technique makes also possible to determine retention factors and solubilities of the compounds. The typical response from this method is presented in Figure 3 [35,44].

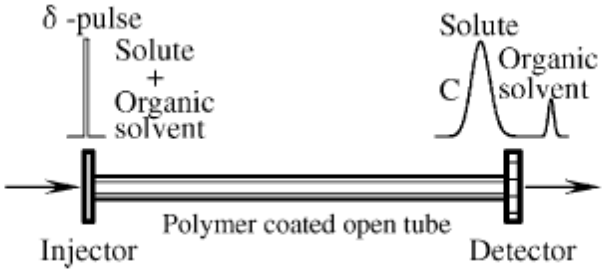

Figure 3 – Typical response of the CIR method to an impulse input signal [35].

Similarly to the CPB method, when a straight pulse is introduced into a laminar solvent stream the solute concentration profile is described by the Eq.2. However the boundary conditions are [42,53]:

$$k\frac{\partial C_2}{\partial t} = -\frac{2D_{12}}{R}\frac{\partial C_2}{\partial r} \text{ for } r = R \quad \text{(Eq.31)}$$

$$\frac{\partial C_2}{\partial r} = 0 \text{ for } r = 0 \quad \text{(Eq.32)}$$

$$C_2 = 0 \text{ for } z = \pm\infty \quad \text{(Eq.33)}$$

where k is the retention factor in the column, which is not influenced by the axial and radial dispersion, but by temperature and pressure. It is also considered that the equilibrium of the solute, between the solvent and the polymer is instantaneous. The retention factor can be determined by one of two ways: by the retention time using Eq.34 or by moment analysis by applying the first and second moments and using the solvent velocity [35].

$$k = \frac{t_{tr}-t_0}{t_0} \quad \text{(Eq.34)}$$

here, t_{tr} is the retention time of the solute and t_0 the retention time of inert species. The initial condition for the current case is:

$$C_2 = \frac{m}{\pi R^2}\frac{\delta(z)}{1+k} \text{ at } t = 0 \quad \text{(Eq.35)}$$

The approximated differential equation of Golay for the average concentration of solute is given by [36,44]:

$$\frac{\partial C^{app}}{\partial t} = a\frac{\partial^2 C^{app}}{\partial z'^2} - b\frac{\partial^2 C^{app}}{\partial z'\partial t} \quad \text{(Eq.36)}$$

where a, b, z and U are defined by:

$$a = \frac{D_{12}}{1+k} + \frac{1+6k+11k^2}{(1+k)^3}\frac{R^2U^2}{48D_{12}} \quad \text{(Eq.37)}$$

$$b = \frac{R^2U^2}{24D_{12}}\frac{k(1+4k)}{1+k} \quad \text{(Eq.38)}$$

$$z' = z - Ut \quad \text{(Eq.39)}$$

$$U = \frac{\bar{u}}{1+k} \quad \text{(Eq.40)}$$

Assuming that $b = 0$, Eq.36 becomes [36]:

$$\frac{\partial C^{app}}{\partial t} = a\frac{\partial^2 C^{app}}{\partial z'^2} \quad \text{(Eq.41)}$$

with initial and boundary condition:

$$C^{app} = \frac{m}{\pi R^2}\frac{\delta(z')}{1+k} \text{ at } t = 0 \quad \text{(Eq.42)}$$

$$C^{app} = 0 \text{ at } z' = \pm\infty \quad \text{(Eq.43)}$$

By solving the previous equation, one obtains the Gaussian like solution given by [36]:

$$C^{app}(z,t) = \frac{m}{\pi R^2}\frac{1}{(1+k)\sqrt{4\pi at}}\exp\left\{-\frac{(z-Ut)^2}{4at}\right\} \text{ for } z,t > 0 \quad \text{(Eq.44)}$$

Adopting the fitting method, k and D_{12} are determined by minimizing ε calculated by Eq.30 where $C^{app}(L,t)$ is the radial average concentration at $z = L$. Regarding the analysis of the chromatographic peak, the same criteria discussed earlier for the case of CPB method

(Chapter 2.1) should be adopted [35]. The value of D_{12} is determined by Eq.45, being this valid under the same conditions as Eq.22 [36].

$$D_{12} = \left[\frac{1+6k+11k^2}{1+k}\right]\left[\frac{\left(R^2\left(\frac{\bar{u}}{1+k}\right)^2\right)}{24a}\right]\Bigg/\left(1+\sqrt{1-\left[\frac{1+6k+11k^2}{(1+k)^2}\frac{R^2\left(\frac{\bar{u}}{1+k}\right)^2}{12a^2}\right]}\right) \quad \text{(Eq.45)}$$

When applying the moment method σ^2 and $\bar{t}$ are determined by the Eq.46 and 47 [36].

$$\bar{t} = \frac{\int_0^\infty tC^{app}(L,t)\mathrm{d}t}{\int_0^\infty C^{app}(L,t)\mathrm{d}t} = \frac{L}{U}\left(1+2\frac{a}{LU}\right) \quad \text{(Eq.46)}$$

$$\sigma^2 = \frac{\int_0^\infty (t-\bar{t})^2 C^{app}(L,t)\mathrm{d}t}{\int_0^\infty C^{app}(L,t)\mathrm{d}t} = 2\left(\frac{L}{U}\right)^2\frac{a}{LU}\left(1+4\frac{a}{LU}\right) \quad \text{(Eq.47)}$$

The retention factor, *k*, can be calculated by [36]:

$$k = \frac{2\left(1-\frac{\sigma^2}{\bar{t}^2}\right)}{3+\sqrt{1+4\frac{\sigma^2}{\bar{t}^2}}}\frac{\bar{t}\bar{u}}{L} - 1 \quad \text{(Eq.48)}$$

Finally the diffusion coefficient is estimated by [36]:

$$D_{12} = \frac{2\alpha}{\beta+\sqrt{\beta^2-4\alpha}}L\bar{u} \quad \text{(Eq.49)}$$

where

$$\alpha = \frac{1+6k+11k^2}{(1+k)^2}\frac{R^2}{48L^2} \quad \text{(Eq.50)}$$

$$\beta = \frac{2\frac{\sigma^2}{\bar{t}^2}-1+\sqrt{1+4\frac{\sigma^2}{\bar{t}^2}}}{4\left(2-\frac{\sigma^2}{\bar{t}^2}\right)} \quad \text{(Eq.51)}$$

2.3. Modified Taylor-Aris technique

The modified Taylor-Aris technique results from a combination of the two previous described methods. Experimentally it uses two columns, one with a polymeric coaingt (as in the CIR method) followed by an open column (as in CPB method). This combination results in a separation of the solute and solvent before entering in the open column. The typical chromatographic response of this method is shown in Figure 4 [35].

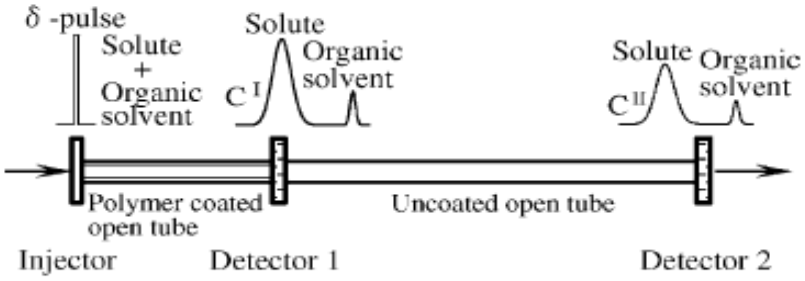

Figure 4 – Typical response for the modified Taylor-Aris method to an impulse input signal [35].

D_{12} is determined by the difference between the variance values at the inlet and the exit of the second column. As in the Taylor-Aris method the concentration profile is described by Eqs.9 and 10, regarding the restrictions to these equation they are [35]:

$$C^{\text{app}} = 0 \text{ for } t = 0 \quad \text{(Eq.52)}$$

$$C^{\text{app}} = C^{\text{I, exp}}(t) \text{ for } z = 0 \quad \text{(Eq.53)}$$

Combining Eqs.9, 10, 52 and 53 with the Eq.12, Eq.55 is obtained:

$$C^{\text{II, app}}(t) = \int_0^t C^{\text{I,exp}}(\xi)\text{f}(t-\xi)\,\text{d}\xi \quad \text{(Eq.54)}$$

F(s) is a function defined by the ratio between the Laplace transform of the exit signal $C^{\text{II, app}}(t)$ and the entry signal $C^{\text{I, app}}(t)$, it is given the Eq.55. By applying the inverse of the Laplace transform to $F(s)$ function, $f(t)$ given by the Eq.56 is obtained [35].

$$F(\text{s}) = \frac{\int_0^\infty C^{\text{II, app}}(t)\text{e}^{-st}\text{d}t}{\int_0^\infty C^{\text{I, app}}(t)\text{e}^{-st}\text{d}t} = \exp\left[\frac{L\bar{u}\left(1-\sqrt{1+4Ds/\bar{u}^2}\right)}{2K}\right] \quad \text{(Eq.55)}$$

$$f(\text{t}) = \frac{L}{\sqrt{4\pi Dt^3}}\exp\left(\frac{-(L-\bar{u}t)^2}{4Dt}\right) \quad \text{(Eq.56)}$$

The present method is suitable to measure binary diffusion coefficient of volatile components as showed by Funazukuri *et al.* [54].

3. Tracer diffusion coefficients models

Several approaches were used to correlate or estimate the tracer diffusivities measured in this work, namely: the Dymond–Hildebrand–Batschinski (DHB) free volume equation [13,55,56]; the predictive tracer diffusion coefficient model of Liu-Silva-Macedo (TLSM) [13,57,58]; the one-parameter correlation of Liu-Silva-Macedo ($TLSM_d$) [13,57,58]; the extension of Liu-Silva-Macedo model to multicomponent systems, using the mixing rules of Merzliak and Pfenning for Lennard-Jones intradiffusivities (LSM-MP) [13,59]; the predictive Wilke-Chang equation [60,61]; a predictive modified Stokes-Einstein equation (mSE_1) [62]; the predictive model of Vaz *et al.* [63]; and four predictive empirical/semi-empirical correlations of Magalhães *et al.* [64]. These models will be briefly described in the next paragraphs.

Model performance was assessed by the average absolute relative deviation, AARD, defined as:

$$\mathrm{AARD}(\%) = \frac{100}{\mathrm{NDP}} \sum_{\mathrm{i}=1}^{\mathrm{NDP}} \left| \frac{D_{12}^{\mathrm{exp}} - D_{12}^{\mathrm{calc}}}{D_{12}^{\mathrm{exp}}} \right|_{\mathrm{i}} \qquad \text{(Eq.57)}$$

where NDP represents the number of points, and D_{12}^{exp} and D_{12}^{calc} are the experimental and calculated values of tracer diffusivities, respectively.

3.1. Dymond–Hildebrand–Batschinski (DHB) correlation

One theory to treat transport properties, (e.g. diffusivities), of dense fluids is that of free volume where the coefficients depend on the relative expansion from an intrinsic molar volume, V_{i}. The importance of these models rely on: Simple equations and reduced number of parameters; Most of the parameters have physical meaning; They are applicable in a vast range of temperature and pressures; The main approaches are based on statistical mechanics giving them a solid background; They can be extended to multicomponent systems [13].

The Dymond–Hildebrand–Batschinski (DHB) it is a free volume model frequently adopted to describe non-polar substances with negligible attractive forces at moderated densities. This model has for based on the work developed by Batschinski for real liquids and later carried over to self-diffusivities by Hildebrand, suggesting a dependency of the diffusion coefficients with the free molar volume. In 1974, the results obtained by Dymond

for hard sphere systems suggested that the equation to be used is Eq.58. In this equation is introduced the dependency on the square root of the temperature [13,55,56]:

$$D_{12} = B_{\mathrm{DHB}}\sqrt{T}(V_{\mathrm{m}} - V_{\mathrm{D}}) \quad \text{(Eq.58)}$$

where V_{m} ($\mathrm{cm^3\ mol^{-1}}$) is the molar volume of the solvent, and V_D ($\mathrm{cm^3\ mol^{-1}}$) and B_{DHB} ($\mathrm{cm^{-1}\ mol\ s^{-1}\ K^{-1/2}}$) are adjustable parameters of the model. V_{D} is the maximum packing volume, meaning it is the minimum molar volume at which diffusivity ceases. Finally B_{DHB} is characteristic of solute-solvent pair [13,55,56]. In some systems the value of V_D may depend on the temperature, and simple relations $\mathrm{V}_D = \mathrm{V}_D(T)$ may be proposed to represent such trend [13,56]. In this work a linear dependency was considered in Chapter 5.4 ($V_{\mathrm{D}} = m_{\mathrm{VD}}T + b_{\mathrm{VD}}$).

Lito *et al.* [65] tested this model in a database with 8293 experimental points from 487 systems (supercritical, liquids and gaseous systems) and was obtained an AARD of 5.22 % [65].

3.2. Predictive model of Tracer-Lui-Silva-Macedo (TLSM)

The Tracer Liu-Silva-Macedo, (TLSM), it is a predictive model (zero parameters). This model has as origin the Liu-Silva-Macedo (LSM) model for self-diffusion coefficients. The reliable results accomplished by this model induced Liu *et al.* [13,57,58] to propose an empirical extension to calculate tracer diffusion, Eq.59.

$$D_{12} = \frac{21.16}{\rho_{\mathrm{n},1}\sigma_{\mathrm{eff},12}^2}\left(\frac{1000R_{\mathrm{g}}T}{M_{12}}\right)^{1/2}\exp\left(-\frac{0.75\rho_1^*}{1.2588\text{-}\rho_1^*} - \frac{0.27862}{T_{12}^*}\right) \quad \text{(Eq.59)}$$

where M_{12} is the reduced molar mass of the system ($\mathrm{g{\cdot}mol^{-1}}$) given by Eq.60, T_{12}^* is the reduced temperature of the system given by Eq.61, $\sigma_{\mathrm{eff},12}$ (cm) is the effective hard sphere diameter of the hard sphere given by Eq.62, $\rho_{\mathrm{n},1}$ ($\mathrm{cm^{-3}}$) is the number density of the solvent given by Eq.64 and ρ_1^* is the reduced density of the solvent given by Eq.63:

$$M_{12} = 2\frac{M_1M_2}{M_1+M_2} \quad \text{(Eq.60)}$$

$$T_{12}^* = \frac{T}{\left(\frac{\varepsilon_{\mathrm{LJ},12}}{k_{\mathrm{B}}}\right)} \quad \text{(Eq.61)}$$

$$\sigma_{\mathrm{eff,i}} = \sigma_{\mathrm{LJ,i}}\times 2^{1/6}\left(1+\sqrt{1.3229T_{\mathrm{i}}^*}\right)^{\text{-}1/6},\ \mathrm{i} = 1,\ 12 \quad \text{(Eq.62)}$$

$$\rho_1^* = \rho_{\mathrm{n},1}\sigma_{\mathrm{eff},1}^3 \quad \text{(Eq.63)}$$

$$\rho_{n,1} = \rho_1 \frac{N_{av}}{M_1} \quad \text{(Eq.64)}$$

where i = 1, 2 or 12 being the last the solute/solvent pair, N_{av} is the Avogadro's number and ρ_1 (g cm^{-3}) is the solvent density. Finally, the two interaction parameters of LJ (energy, $\varepsilon_{LJ,12}/k_B$ (K), and diameter, $\sigma_{LJ,12}$ (cm)), are estimated by the following combining rules:

$$\sigma_{LJ,12} = \frac{\sigma_{LJ,1}+\sigma_{LJ,2}}{2} \quad \text{(Eq.65)}$$

$$\frac{\varepsilon_{LJ,12}}{k_B} = \frac{\sqrt{\frac{\varepsilon_{LJ,1}}{k_b}\sigma_{LJ,1}^3 \times \frac{\varepsilon_{LJ,2}}{k_b}\sigma_{LJ,2}^3}}{\sigma_{LJ,12}{}^3} \quad \text{(Eq.66)}$$

Finally if the LJ energy and diameter of the pure component i is unknown, Eq.67 to 69 should be used to estimate them [58]:

$$\frac{\varepsilon_{LJ,i}}{k_B} = 0.774 T_{c,i} \text{ , i} = 1,2 \quad \text{(Eq.67)}$$

$$\sigma_{LJ,i}^3(\text{Å}) = 0.17791 + 11.779 \frac{T_{c,i}}{P_{c,i}} - 0.049029 \left(\frac{T_{c,i}}{P_{c,i}}\right)^2, \ \frac{T_{c,i}}{P_{c,i}} \leq 100 \quad \text{(Eq.68)}$$

$$\sigma_{LJ,i}^3(\text{Å}) = 0.809 V_{c,i}^{1/3}, \ \frac{T_{c,i}}{P_{c,i}} > 100 \quad \text{(Eq.69)}$$

where the subscript c identifies a critical property.

Magalhães *et al.* [58] tested this model in a database containing 5279 experimental points (supercritical, liquids and gaseous systems) from 296 binary systems and worth an AARD of 15.71 % was obtained.

It is worth noting that the present model cannot be applied to hydrogen bonding solvents like alcohols and water. The TLSM model is based on Lennard-Jones potential which accounts for van der Waals forces, which are much weaker than those that prevail in solvents with hydrogen bond and dipole-dipole interactions [13,57,66].

3.3. 1-parameter correlation of Tracer-Liu-Silva-Macedo (TLSM$_d$)

The TLSM$_d$ is a one parameter model generated from the TLSM model by inserting the interactions constant $k_{12,d}$ into the diameter combining rule. This constant is an adjustable parameter of the model. Hence, the binary LJ parameters, diameter and energy, are [13,57,58]:

$$\sigma_{LJ,12} = \left(1 - k_{12,d}\right) \frac{\sigma_{LJ,1}+\sigma_{LJ,2}}{2} \quad \text{(Eq.70)}$$

$$\frac{\varepsilon_{LJ,12}}{k_b} = 8 \frac{\sqrt{\frac{\varepsilon_{LJ,1}}{k_b}\sigma_{LJ,1}^3 \times \frac{\varepsilon_{LJ,2}}{k_b}\sigma_{LJ,2}^3}}{\left(\sigma_{LJ,1}+\sigma_{LJ,2}\right)^3} \quad \text{(Eq.71)}$$

Similarly to the previous models this was also tested by Magalhães *et al.* [58] with the same database obtaining an AARD of 3.89 %, a smaller error when compared with TLSM.

TLSM and $TLSM_d$ models were both designed for the calculation of D_{12} in binary systems at infinite dilution. Therefore, their application to a ternary system (e.g. eucalyptol/SC-CO_2/ethanol) may be accomplished after defining a pseudo-component representative of the solvent mixture. The following methodology has been adopted to calculate D_{12}: (i) The critical properties of the solvent mixture were estimated using the correlations of Chueh and Prausnitz, Schick and Prausnitz, and Kreglewski and Kay [61] (the values of the critical properties can be consulted in Table 3 of Chapter 5.5 and the correlations in Appendix B); (ii) the LJ energy and diameter parameters were estimated by Eqs.67 to 69 considering the solvent mixture as a pseudo-component; (iii) D_{12} values were evaluated as usually using TLSM and $TLSM_d$ models.

3.4. Extension of Liu-Silva-Macedo model to multicomponent LJ intradiffusivities using mixing rules of Merzliak and Pfenning (LSM-MP)

The extension of the Liu-Silva-Macedo model to multicomponent systems was firstly accomplished by Merzliak and Pfenning [13,59], who studied intradiffusivities of Lennard-Jones mixtures, $D_{i,LJ}$. The model embodies five constants (that were optimized using molecular dynamics data) and includes six mixing rules. The final expressions are:

$$D_{i,LJ} = \frac{21.16}{\rho_n \sigma_{mix,i}^2}\left(\frac{1000 R_g T}{M_{eff,i}}\right)^{1/2} \exp\left(-\frac{\theta_4 \rho_{eff,i}^*}{\theta_2 - \rho_{eff,i}^*} - \frac{\theta_3}{T_{mix,i}^*}\right) \quad \text{(Eq.72)}$$

$$\rho_{eff,i}^* = \rho \sigma_{mix,i}^a \sigma_{mix,i}^b \quad \text{(Eq.73)}$$

$$\sigma_{mix,i}^a = \sum_{j=1}^{N} x_j \sigma_{eff,i,j}^{\ 1-\theta_1} \quad \text{(Eq.74)}$$

$$\sigma_{mix,i}^b = \sum_{i=1}^{N} \sum_{j=1}^{N} x_i x_j \sigma_{eff,i,j}^{\ \theta_1} \quad \text{(Eq.75)}$$

$$\sigma_{mix,i}^2 = \sum_{j=1}^{N} x_j \sigma_{eff,i,j}^{\ 2} \quad \text{(Eq.76)}$$

$$\sigma_{eff,i,j} = \sigma_{LJ,i,j} \times 2^{1/6}\left(1 + \sqrt{\frac{T_{eff,i,j}^*}{\theta_5}}\right)^{-1/6} \quad \text{(Eq.77)}$$

$$T_{eff,i,j}^* = \frac{T}{\left(\frac{\varepsilon_{LJ,i,j}}{k_b}\right)} \quad \text{(Eq.78)}$$

$$T_{mix,i}^* = \sum_{j=1}^{N} x_j T_{eff,i,j}^* \quad \text{(Eq.79)}$$

$$m_{\mathrm{eff,i}}^{-1/2} = \frac{1}{2}\sum_{\mathrm{j=1}}^{\mathrm{N}} x_{\mathrm{j}}\left(m_{\mathrm{i}}^{-1/2} + m_{\mathrm{j}}^{-1/2}\right) \quad \text{(Eq.80)}$$

$$M_{\mathrm{eff,i}} = N_{\mathrm{av}} m_{\mathrm{eff,i}} \quad \text{(Eq.81)}$$

where the subscripts i, j = 1,..,N span all components of the mixture (N), m_{i} is the mass of molecule i, $\sigma_{\mathrm{LJ,i,i}}$ and $\varepsilon_{LJ,i,i}/\mathrm{k_B}$ are the LJ parameters of pure component i, $\sigma_{\mathrm{LJ,i,j}}$ and $\varepsilon_{\mathrm{LJ,i,j}}/\mathrm{k_B}$ are the cross LJ parameters, x_{i} is the molar fraction of i, ρ_{n} is the number density of the mixture, $\rho^{*}_{\mathrm{eff,i}}$ is the effective reduced density based on component i, $T^{*}_{\mathrm{eff,i,j}}$ is the effective reduced temperature based on pair ij, $m_{\mathrm{eff,i}}$ is an effective mass of component i in the mixture, and finally θ_{j} (j=1 to 5) are model constants (θ_1 = 2.159807; θ_2 = 1.156846; θ_3 = 0.414496; θ_4 = 0.610344; θ_5 = 0.564022) [13,59].

3.5. Wilke-Chang equation

The Wilke-Chang method is based on the Stokes-Einstein relation that establishes that:

$$D_{12} = \frac{R_{\mathrm{g}} T}{6\pi\mu_1 r_2} \quad \text{(Eq.82)}$$

where r_2 it is the radius of the spherical solute and μ_1 the solvent viscosity. Eq.82 is strictly applied to macroscopic systems [61].

The Wilke-Chang is an empirical modification of the Stokes-Einstein relation. Although it is an old predictive model it is still widely used. For binary systems the model is given by [60,61]:

$$D_{12} = 7.4 \times 10^{-8} \frac{(\Phi M_1)^{1/2} T}{\mu_1 V_{\mathrm{TC,bp,2}}^{0.6}} \quad \text{(Eq.83)}$$

$$V_{\mathrm{TC,bp,i}} = 0.285 \times V_{\mathrm{c,i}}^{1,048} \quad \text{(Eq.84)}$$

where Φ is the association factor of the solvent (e.g., 2.6 for water, 1.9 for methanol, 1.5 for ethanol, and 1.0 for non-associating solvents), and $V_{\mathrm{TC,bp,2}}$ is the solute molar volume at its normal boiling point, here estimated by the method of Tyn and Calus (Eq.84) [61]. In the case of solvent mixtures, the Wilke-Chang equation can also be applied if μ_1 is substituted by the viscosity of the mixture, and parameter ΦM_1 is estimated by:

$$\Phi M_1 = \sum_{\mathrm{i=1}}^{\mathrm{N}} x_{\mathrm{i}} \Phi_{\mathrm{i}} M_{\mathrm{i}} \quad \text{(Eq.85)}$$

This model was tested by Lito *et al.* using the same data base as in Chapter 3.5 and AARD = 20.74 % was achived [65].

3.6. Lai-Tan equation foe SC-CO_2 systems

The Wilke-Chang equation was modified by Lai-Tan [48] to account for the nonlinear dependency of D_{12} on $1/\mu_1$. The final expression is:

$$D_{12} = 2.50\times10^{-7}\frac{(M_1)^{1/2}T}{(10\times\mu_1)^{0.688}V_{c,2}^{1/3}} \quad \text{(Eq.86)}$$

where $V_{c,2}$ is the critical volume of the solute. It is important to mention that this equation was devised for supercritical carbon dioxide systems [63].

3.7. Modified Stokes-Einstein-1 (mSE$_1$) equation of Magalhães *et al.* [62]

The Modified Stokes-Einstein-1, mSE$_1$, is a hydrodynamic model for diffusion coefficients in SC-CO_2, developed by Magalhães *et al.* [62] and based on the Stokes-Einstein expression. The model equation in CGS units with viscosity in cP is:

$$D_{12} = 1.1335\times10^{-6}\left(\frac{T}{\mu_1}\right)^{0.8468}\frac{1}{\left(M_2V_{bp,2}^{exp}\right)^{0.2634}} \quad \text{(Eq.87)}$$

$$V_{bp,2}^{exp} = 1.459\left(V_{TC,bp,2}\right)^{0.894} \quad \text{(Eq.88)}$$

where $V_{TC,bp,i}$, is the molar volume of component *i* at its normal boiling point estimated by the method of Tyn and Calus (see Eq.84).

3.8. Predictive model of Vaz *et al.* [63] for D_{12} SC-CO_2

The present model was developed by Vaz *et al.* [63] to estimate tracer diffusion coefficients in SC-CO_2. The model combines two terms, background (D_{12}^{b}) and singular (D_{12}^{s}), with the objective to represent D_{12} accurately not only far but also near the critical point. The model is:

$$D_{12} = D_{12}^{b} + D_{12}^{s} = A\left(\frac{T}{\mu_1}\right)^{\alpha}\frac{1}{\left(M_2V_{bp,2}\right)^{\beta}} + \frac{k_BT}{6\pi\mu_1\sigma_{12}}\left[\frac{1}{1+\theta\left(1-\frac{1}{2}\Gamma_{12}^{\infty}\right)^{1/2}}\right] \quad \text{(Eq.89)}$$

where α=0.8140, β=0.2530, A=3.247×10^{-7} and θ=8.570, k_B is the Boltzmann's constant (1.38065x10^{-16} erg K^{-1}), and Γ_{12}^{∞} is a thermodynamic factor at infinite dilution calculated on the basis of Peng-Robinson equation of state (further details in [63]).

3.9. Simple empirical and semi-empirical correlations Magalhães *et al.* [64]

Magalhães *et al.* [64] developed several empirical and semi-empirical correlations that relate the diffusion coefficient with temperature, T (K), solvent viscosity, μ_1 (cP) and solvent density, ρ_1 (g·cm^{-3}). These equations are very simple and possess two adjustable parameters, a_i and b_i.They can be divided in four groups: Group 1 relates the D_{12} with temperature and solvent viscosity; Group 2 shows that the D_{12} depends only on the viscosity of the solvent; Group 3 shows the dependency of the D_{12} with the temperature and density on the solvent; Group 4 combined the influence of temperature with density and solvent viscosity. For this work one equation from each group was selected:

$$\ln\frac{D_{12}}{T} = a_1 \ln\mu_1 + b_1 \quad \text{(Eq.90)}$$

$$D_{12} = a_2\frac{1}{\mu_1} + b_2 \quad \text{(Eq.91)}$$

$$\frac{D_{12}}{T} = a_3\rho_1 + b_3 \quad \text{(Eq.92)}$$

$$\frac{D_{12}}{T} = a_4\rho_1 + \frac{b_4}{\mu_1} \quad \text{(Eq.93)}$$

4. Experimental Section

This chapter includes the chemical compounds used in this work, equipment description, experimental procedure and conditions for D_{12} determination. Moreover, the models for the solvent estimation properties (density and viscosity), later required for data interpretation and modelling.

4.1. Chemicals

Eucalyptol (CAS number 470-82-6) with purity 100 % was provided by José M. Vaz Pereira Ltd., carbon dioxide (CAS number 124-38-9) with purity 99.999 % (v/v) was purchased from Praxair, and absolute ethanol (CAS number 64-17-5) was supplied by Fisher Chemical. All chemicals were used without further purification.

4.2. Equipment and experimental procedure

A scheme of the experimental apparatus used to measure the diffusion coefficients by the CPB technique is presented in Figure 5. The solvents were pumped from the reservoirs (1) and (5) at constant flow rate using the syringe pumps (2) and (4), namely a Teledyne ISCO model 260D with 266.06 cm^3 capacity for CO_2 and a Teledyne ISCO model 100 DM 102.97 cm^3 capacity for liquid ethanol. The CO_2 pump (2) was coupled with a Julabo F12 thermostatic bath (3) set to 21.0 °C, to avoid temperature oscillations that would cause flow rate fluctuations during experiments. The solvents were pre-heated in a stainless-steel column (7) placed inside a LSIS-B2V/IC 22 oven (Venticell, MMM Group) and fed to an open capillary column (8) (PEEK tubing, with R = 0.261 mm, L = 10.243 m and R_c = 0.150 m) connected to a UV-vis detector (10) (UV Detector 2500, Knauer) set at a system-specific wavelength (see Chapter 5.1). After reaching steady-state conditions (constant pressure, temperature and baseline during 1-2 h after start-up) a small volume of solute (0.1 μL) was injected in a short period (pulse input) using a C74H-1674 injector (6) from Valco Instruments Co. Inc.. The outlet pressure was controlled by a Jasco BP-2080 back pressure regulator (12) and the volumetric flow rate was measured with a soap-bubble flow meter (13).

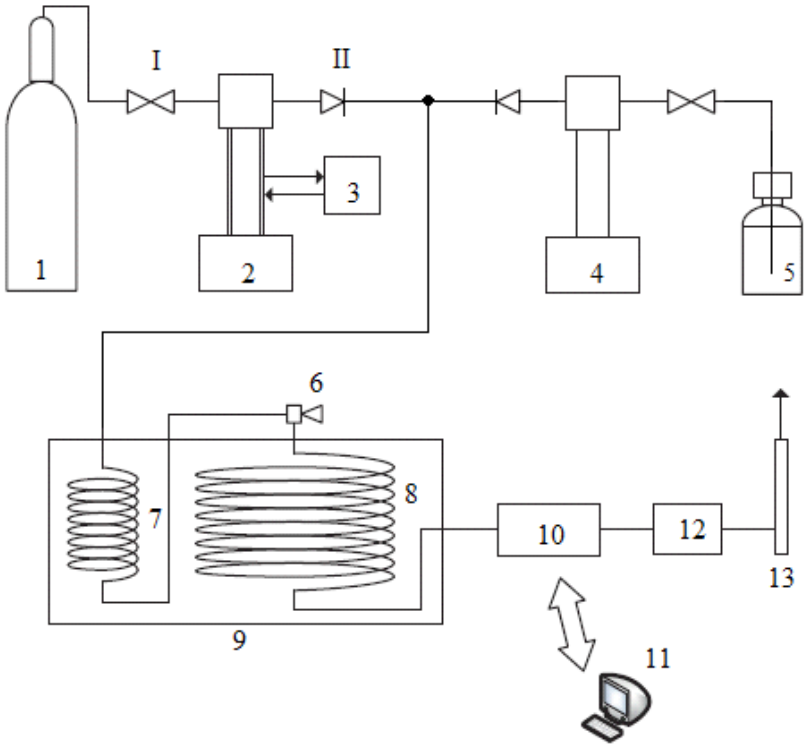

Figure 5 – Scheme of the experimental apparatus used to measure tracer diffusion coefficients in liquid or supercritical fluids: (1) CO_2 cylinder, (2) CO_2 syringe pump, (3) thermostatic bath, (4) ethanol syringe pump, (5) ethanol reservoir, (6) injector, (7) pre-heating column, (8) diffusion column, (9) oven, (10) UV-vis detector, (11) data acquisition software, (12) back pressure regulator – BPR, (13) soap-bubble flow meter, (I) on/off valves, and (II) check valves.

4.3. Experimental conditions of D12 measurement

The diffusion coefficient of eucalyptol was measured in SC-CO_2 modified with 8 wt.% ethanol (eucalyptol/SC-CO_2/ethanol) and in pure liquid ethanol (eucalyptol/ethanol). The experimental conditions in the case of eucalyptol/SC-CO_2/ethanol were 303.15, 313.15, 323.15 and 333.15 K, and pressures of 150, 175, 200, 225, 250 and 275 bar, at a wavelength of 220 nm (see Chapter 5.1). For the binary system eucalyptol/ethanol, the assays were carried out at 303.15, 313.15, 323.15 and 333.15 K, and pressures of 1, 50 and 100 bar, at a wavelength of 200 nm (see Chapter 5.1). More information about the solvents can be found in Appendix A.

4.4. Solvent properties

In order to analyze the measured diffusion coefficients it was necessary to estimate the solvent properties, in this particular case density and viscosity. The methods/models used

are described in the following; all of them were previously validated in a previous work carried out under similar conditions [67].

- **Density of liquid ethanol**

The pure liquid ethanol density was calculated using the Tait [68] equation:

$$\frac{\rho-\rho_0}{\rho} = 0.2000\times\log\left(\frac{B+P}{B+P_0}\right) \quad \text{(Eq.93)}$$

$$B = 520.23\text{-}1240\times\frac{T}{T_C}+827\times\left(\frac{T}{T_C}\right)^2 - F \quad \text{(Eq.94)}$$

where ρ and ρ_0 are densities at the corresponding pressures P and P_0, and F for ethanol is 0.72, (calculated by Eq.95, where C_n is the number of carbons of the molecule). The density at atmospheric pressure (ρ_0) is calculated according to the Eykman method as suggested by Cano-Gómez *et al.* [69].

$$F = 0.015\times C_n\times(1+11.5\times C_n) \quad \text{(Eq.95)}$$

$$\rho_0 = \frac{n_D^2-1}{n_D+0.4}\frac{1}{K} \quad \text{(Eq.96)}$$

where n_D and K are the refractive index and a characteristic constant, respectively, given by:

$$K = 0.72719 - 0.39294\exp(C_n^{-0.89255}\times 0.47272) \quad \text{(Eq.97)}$$

$$n_D = a_0+a_1C_n^{a_2}+a_3C_n+\frac{a_4}{C_n^{a_5}}+\left(a_6+a_7C_n^{0.5}+a_8C_n^{0.75}\right)\times T(°C) \quad \text{(Eq.98)}$$

where a_0=1.87961; a_1=0.55029; a_2=−0.11935; a_3=−0.00161; a_4=0.01344; a_5=13.54426; a_6=−0.00043235; a_7=0.00000954; a_8=0.0000022.

- **Viscosity of liquid ethanol**

Cano-Gómez *et al.* [70] suggested using the Mamedov equation (Eq.99) for determining ethanol viscosity at high pressures:

$$\frac{\mu}{\mu_0} = \left(\frac{\rho}{\rho_0}\right)^A \quad \text{(Eq.99)}$$

where A is given by:

$$A = 10.4+0.0006C_n^{3.5} - \frac{5}{C_n} \quad \text{(Eq.100)}$$

and μ_0 is given by Eq.101 [71]:

$$\log\mu_0 = A + \frac{B}{T} + C\times T + D\times T^2 \quad \text{(Eq.101)}$$

where A=0.72719; B=−0.39294; C=−0.89255; D=0.47272.

- **Density of the SC-CO_2/ethanol mixtures**

The density of the mixture SC-CO_2/ethanol was calculated using the Soave-Redlich-Kwong equation of state (Eq.102-109) as suggested by Kariznovi *et al.* [72].

$$P = \frac{R_g T}{V_m - b} - \frac{a(T)}{V_m^2 + V_m b} \quad \text{(Eq.102)}$$

$$a(T) = \alpha(T)\left[\frac{R_g^2 T_c^2}{P_c} \times 0.42747\right] \quad \text{(Eq.103)}$$

$$b = \frac{R_g T_c}{P_c} \times 0.08664 \quad \text{(Eq.104)}$$

$$\alpha(T) = \left(1 + k\left[1 - \left(\frac{T}{T_c}\right)^{1/2}\right]\right)^2 \quad \text{(Eq.105)}$$

$$k = 0.480 + 1.574\omega - 0{,}176\omega^2 \quad \text{(Eq.106)}$$

$$a_m = \sum_i x_i D_i \quad \text{(Eq.107)}$$

$$b_m = \sum_i x_i b_i \quad \text{(Eq.108)}$$

$$D_i = \sqrt{a_i} \sum_j x_j (1 - \delta_{ij}) \sqrt{a_j} \quad \text{(Eq.109)}$$

where ω is the acentric factor and δ_{ij} is the binary interaction parameter. For the mixture ethanol/CO_2 δ_{ij} = 0.0789 [72].

- **Viscosity of SC-CO_2/ethanol mixtures.**

The viscosity of the mixture SC-CO_2/ethanol can be calculated by the mixing relation described by Kendall and Monroe [73]:

$$\mu_{mix} = \left(x_{ethanol} \times \mu_{ethanol}^{1/3} + x_{CO_2} \times \mu_{CO_2}^{1/3}\right)^3 \quad \text{(Eq.110)}$$

where the viscosity of the CO_2, for this work, was calculated using the Altunin and Sakhabetdinov empirical expression [74].

5. Results and discussion

This Chapter presents the optimization of experimental procedures (Chapter 5.1), the experimental results for tracer diffusion coefficients of eucalyptol in SC-CO_2 modified with ethanol 8 wt.% (Chapter 5.2) and in pure ethanol (Chapter 5.3), the analysis of the measured data by several models (Chapter 5.4) and finally the results of the modeling of a ternary systems database in Chapter 5.5.

5.1. Optimization of the experimental conditions

The tracer injection response curves were registered at the end of the diffusion capillary column using a UV-vis detector set at a precise wavelength (λ) optimized for eucalyptol detection with minimum experimental noise and error. For this purpose, a sample of eucalyptol was analyzed in a UV-vis spectrophotometer, revealing a large peak with maximum absorbance at 220 nm. Thereafter, several eucalyptol diffusion assays were performed under similar conditions (SC-CO_2 modified with 8 wt.% ethanol, 150 bar and 323.15 K) and recording the response curves at different wavelengths (in the range 200 - 225 nm). The preliminary results of D_{12} (calculated with Eqs.10, 13 and 30) and the corresponding root mean square errors, ε, are plotted against wavelength in Figure 6. It can be concluded that λ=220 nm ensures: lower fitting errors (ε =1.09 % average of three replicates); small D_{12} variations upon wavelength perturbation (i.e., stable region); and very reproducible results. Similar tests performed for the binary system (eucalyptol in pure liquid ethanol) disclosed an optimum at λ=200 nm (results shown in Figure 7).

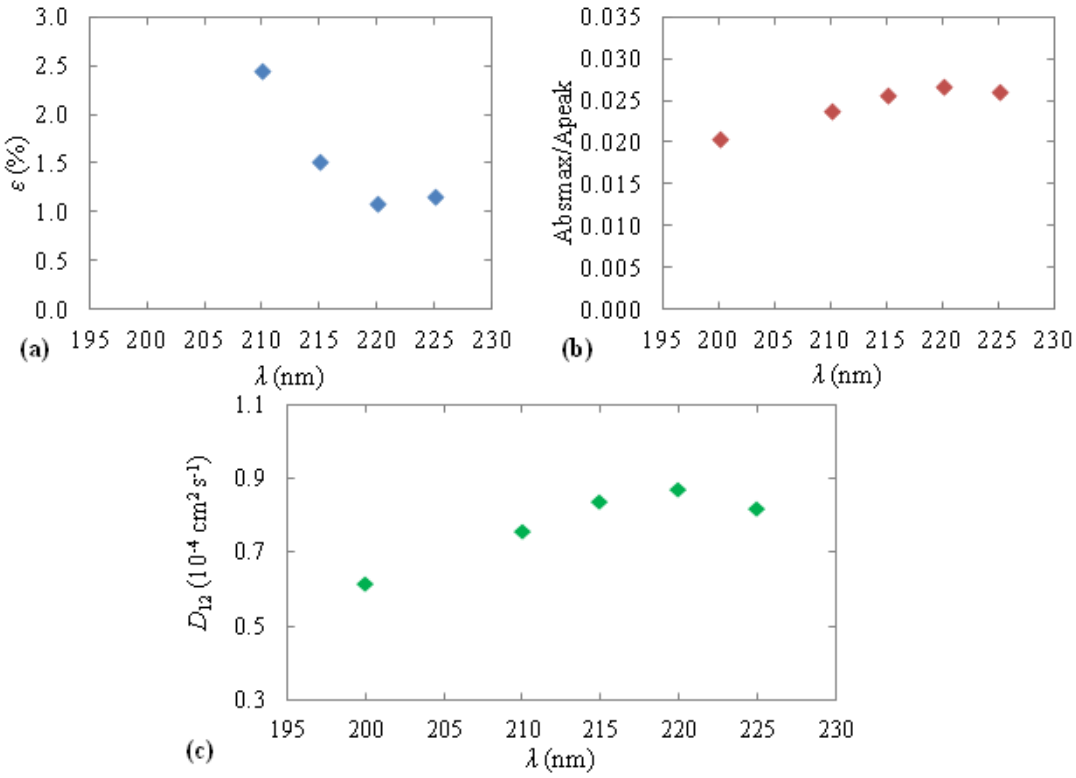

Figure 6 – Identification of the best wavelength (λ, nm) to record the response curves of eucalyptol in SC-CO_2 modified with 8 wt.% ethanol, at 150 bar and 323.15 K; (a) Root mean square error *versus* λ; (b) Ratio of maximum absorbance to peak area (Abs_{max}/A_{peak}) *versus* λ; and (c) preliminary D_{12} results *versus* λ. Then final wavelength selected was 220 nm.

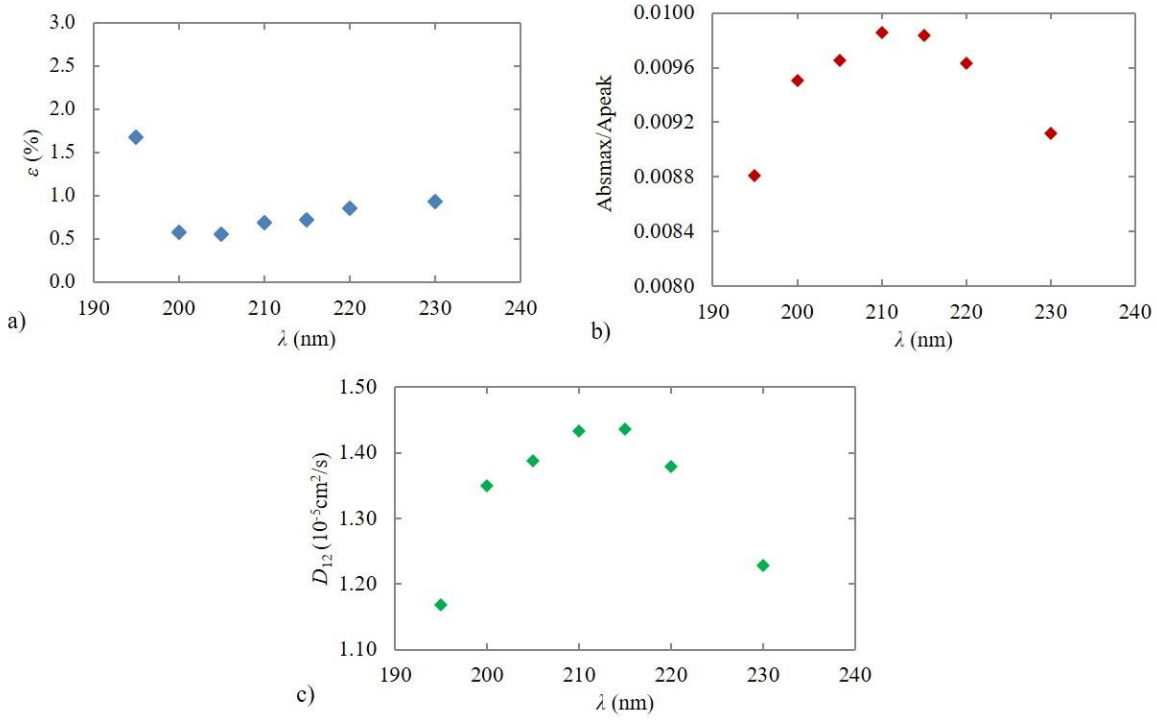

Figure 7 – Identification of the best wavelength (λ, nm) to record the response curves of eucalyptol in pure liquid ethanol, at 1 bar and 323.15 K; (a) Root mean square error *versus* λ; (b) Ratio of maximum absorbance to peak area (Abs_{max}/A_{peak}) *versus* λ; and (c) preliminary D_{12} results *versus* λ. Then final wavelength selected was 200 nm.

The concentration of the injected solute is another important aspect of the experimental procedure, and it has been also considered in this work. In fact, small amounts of solute should be injected in order to get concentration-independent diffusivities and to satisfy the underlying principle of CPB method, i.e. approximately infinite dilution of the solute inside the column. The preliminary experiments performed with ethanol solutions of eucalyptol (23 and 54 %, w/w) delivered unsatisfactory responses, with small peaks easily mistaken with experimental noise. When pure eucalyptol was injected, the response curves were reliable and the D_{12} measurements consistent. In this work, only 0.1 μL of eucalyptol was always injected.

A typical response curve for the ternary system eucalyptol/SC-CO_2/ethanol, at 200 bar and 333.15 K, is illustrated in Figure 8. Similar response curves were obtained throughout the work, with almost no peak tailing effects, reason why the diffusivities obtained by the fitting method (Eqs.10, 13 and 30) were very similar to those calculated by the peak variance method (Eqs.22 and 23).

Finally, the applicability of the CPB method was confirmed for both systems with the constraints previously listed in Section 2.1 being observed, namely: (i) the solvent flow was laminar with Re in the range 46-129 for SC-CO_2/ethanol, and 6-13 for pure ethanol; (ii) the peaks were approximately Gaussian ($D/\bar{u}L < 0.000361$ for SC-CO_2/ethanol and $D/\bar{u}L < 0.00177$ for pure ethanol); (iii) secondary flow effects associated to coiled columns were negligible ($DeSc^{0.5}$ always inferior to 10 in both systems); (iv) the root mean square errors, ε, were small (0.41-1.10 % for SC-CO_2/ethanol and 0.54-0.80 % for pure ethanol); (vi) the asymmetric factors, S_{10}, were close to one (1.01-1.16 for SC-CO_2/ethanol and 1.05-1.19 for pure ethanol).

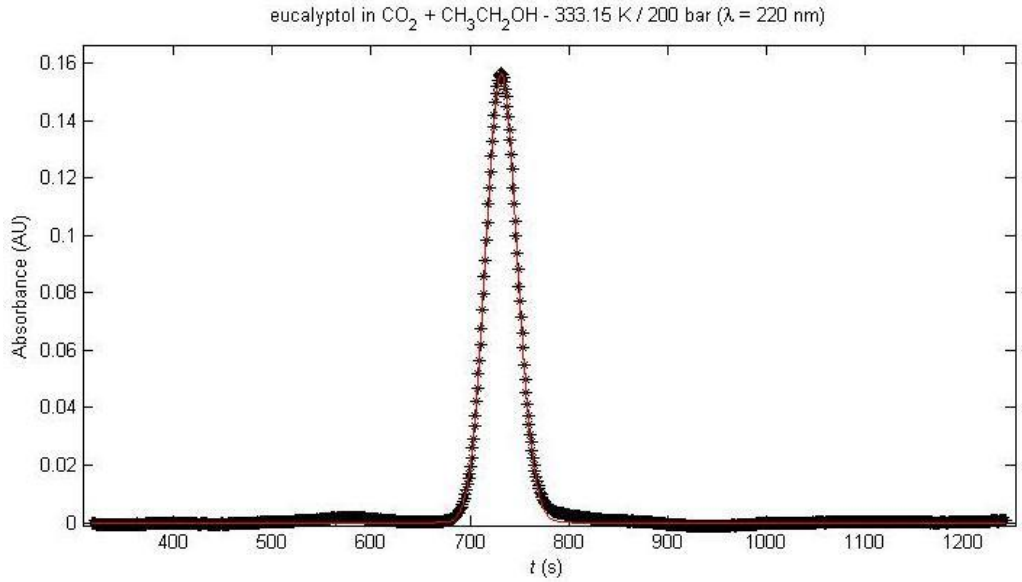

Figure 8 – Typical experimental (*) and calculated (-) response curve (λ=220 nm) for the ternary system eucalyptol/SC-CO_2/ethanol (8 wt.%) at 333.15 K and 200 bar.

5.2. Tracer diffusivity of eucalyptol in SC-CO_2/ethanol

The measured tracer diffusivities of eucalyptol in SC-CO_2 modified with ethanol (8 wt.%) are presented in Table 1, along with necessary solvent properties, namely: density, ρ_{mix} (estimated with Soave-Redlich-Kwong equation of state [72]), and viscosity, μ_{mix} (computed with the Kendall and Monroe equation [73], and the Altunin and Sakhabetdinov empirical expression [74] for the viscosity of SC-CO_2). The experimental diffusivity results varied between 0.547×10^{-4} and 1.042×10^{-4} cm^2 s^{-1}, for temperatures in the range 303.15-333.15 K and pressure between 150 and 275 bar. The D_{12} values are in the same order of magnitude of others reported for compounds under similar conditions

such as, for example: L-menthone and L-carvone in SC-CO_2 with and without ethanol (5 and 10 mol.%) [75]; L-carvone and geraniol in pure SC-CO_2 and SC-CO_2 modified with alcohols (like methanol and isopropanol, 10 mol.%) [76]; α-pinene and β-pinene in SC-CO_2 [51]; chromium(III) acetylacetonate in SC-CO_2 [17].

Table 1 – Experimental D_{12} values of eucalyptol in SC-CO_2 modified with ethanol (8 wt.%), and calculated density and viscosity of the solvent mixture.

T (K)	P (bar)	$D_{12} \pm \Delta D_{12}$ (10^{-4} cm^2 s^{-1})	ρ_{mix} (g cm^{-3})	μ_{mix} (cP)
303.15	150	0.621±0.017	0.794	0.114
	175	0.593 ± 0.010	0.811	0.120
	200	0.571 ± 0.003	0.827	0.126
	225	0.557 ± 0.006	0.841	0.131
	250	0.552 ± 0.009	0.854	0.136
	275	0.547 ± 0.005	0.866	0.140
313.15	150	0.743 ± 0.014	0.746	0.097
	175	0.696 ± 0.014	0.767	0.104
	200	0.642 ± 0.013	0.786	0.110
	225	0.629 ± 0.004	0.803	0.115
	250	0.611± 0.010	0.818	0.121
	275	0.597 ± 0.003	0.832	0.125
323.15	150	0.859 ± 0.013	0.692	0.081
	175	0.815 ± 0.004	0.719	0.089
	200	0.765 ± 0.016	0.743	0.096
	225	0.730 ± 0.019	0.762	0.102
	250	0.703 ± 0.011	0.780	0.107
	275	0.689 ± 0.009	0.796	0.112
333.15	150	1.042 ± 0.024	0.632	0.066
	175	0.935 ± 0.017	0.668	0.076
	200	0.871 ± 0.011	0.696	0.084
	225	0.828 ± 0.020	0.720	0.090
	250	0.772 ± 0.010	0.741	0.095
	275	0.747 ± 0.015	0.759	0.100

Data presented in Table 1 and Figure 9 illustrates the pressure dependence of D_{12} at constant temperature. For each isotherm, the diffusion coefficient decreases with increasing pressure and this is explained by the increment of solvent density, which reduces the free volume available for solute movement. Furthermore, since the solvent molecules are more tightly packed the solute needs more energy to escape from the force

field generated by them (i.e., it is increasingly more difficult for the solute molecules to diffuse across the solvent) [66,77,78]. From these results, it is explicit that the pressure dependency is influenced by temperature with changes in D_{12} being more noticeable at higher temperatures. This behavior is related to pronounced changes in viscosity and density in the high temperature region. Regarding the influence of temperature on the diffusion coefficient of the solute under isobaric conditions, it has a positive effect due to the increase of internal energy (notably kinetic energy) and free volume of the system [78]. Both trends observed under isothermal and isobaric conditions are totally consistent with results reported by other researchers [75,79–83].

The dependence of D_{12} on solvent density is illustrated in Figure 10. The negative effect of density is evident and can be explained by the increasing number of collisions between solute and solvent molecules (owing to the shorter average intermolecular distances), which determines a more erratic diffusion path of the solute through the solvent [13,17,51]. In terms of the free volume theory, when density increases the free volume available for solute movement is reduced; besides, the solute needs more energy to overcome the activation energy barrier for diffusion as has been explained above.

The hydrodynamic behavior of our system was also evaluated by representing diffusivity values using Stokes-Einstein coordinates, T/μ_1. The results (Figure 11) exhibit a linear relationship but the non-zero intercept (0.146×10^{-4} cm^2 s^{-1}) indicates a small deviation from hydrodynamic behavior. Similar results have been consistently reported in other studies [33,51,75].

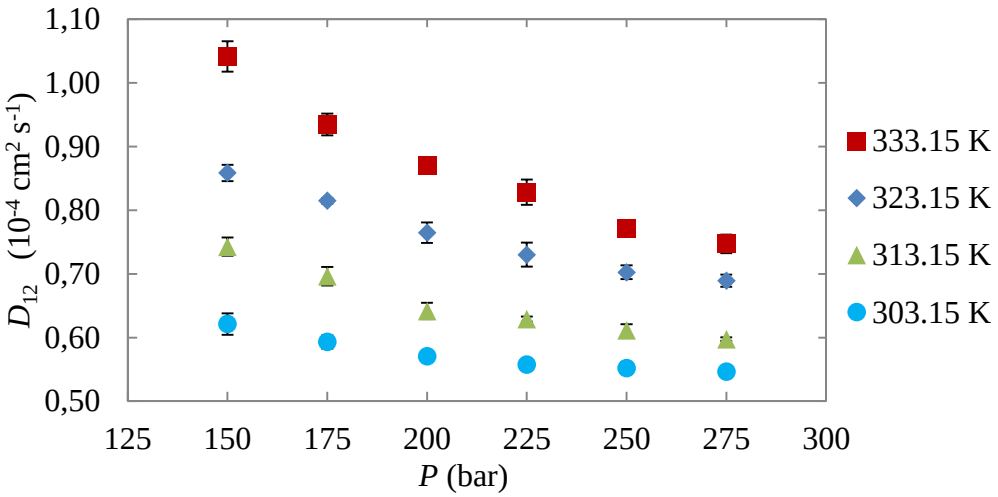

Figure 9 – Tracer diffusion coefficients of eucalyptol in SC-CO_2 modified with ethanol (8 wt.%) as function of pressure at different temperatures.

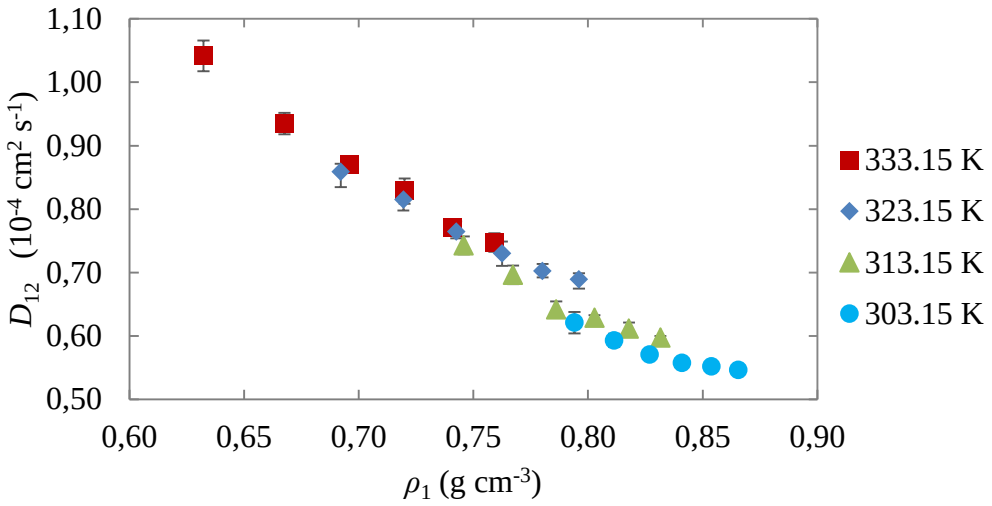

Figure 10 – Tracer diffusion coefficients of eucalyptol in SC-CO_2 modified with ethanol (8 wt.%) as function of solvent density at different temperatures.

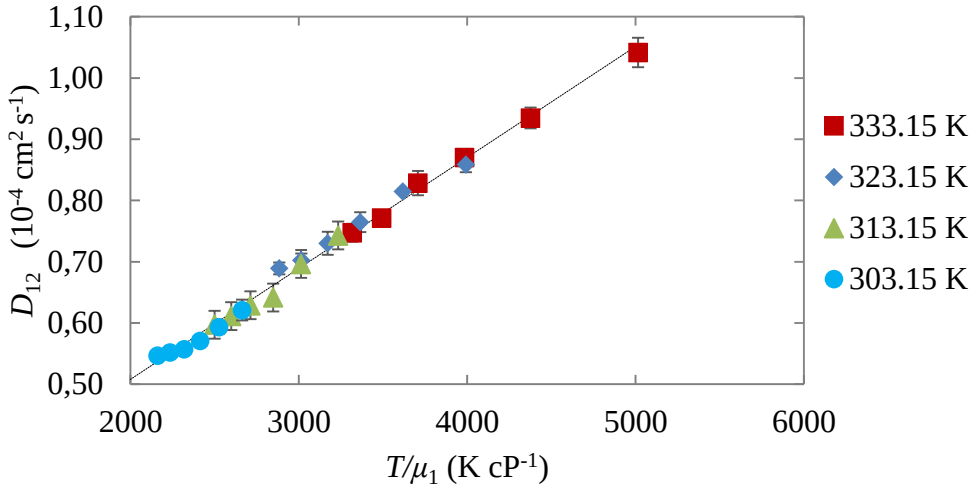

Figure 11 – Tracer diffusion coefficients of eucalyptol in SC-CO_2 modified with ethanol (8 wt.%) plotted in Stokes-Einstein coordinates at different temperatures.

5.3. Tracer diffusivity of eucalyptol in pure liquid ethanol

The experimental results for eucalyptol diffusivity in pure liquid ethanol are presented in Table 2 along with the density and viscosity of ethanol calculated with the Tait equation [68] and the Mamedov equation, respectively [70]. The D_{12} values for eucalyptol in pure ethanol, at temperatures between 303.15 and 333.15 K and pressures between 1 and 100 bar, ranged between 0.912×10^{-5} and 1.578×10^{-5} cm^2 s^{-1}.

Table 2 – Experimental D_{12} values for eucalyptol in pure liquid ethanol, and calculated density and viscosity of the solvent.

T (K)	P (bar)	$D_{12} \pm \Delta D_{12}$ (10^{-5} cm^2 s^{-1})	ρ_1 (g cm^{-3})	μ_1 (cP)
303.15	1	0.981 ± 0.005	0.782	0.965
	50	0.950 ± 0.004	0.791	1.064
	100	0.912 ± 0.003	0.801	1.168
313.15	1	1.162 ± 0.008	0.773	0.810
	50	1.126 ± 0.004	0.783	0.899
	100	1.082 ± 0.002	0.793	0.993
323.15	1	1.349 ± 0.010	0.764	0.687
	50	1.295 ± 0.002	0.775	0.767
	100	1.266 ± 0.003	0.785	0.852
333.15	1	1.578 ± 0.022	0.756	0.587
	50	1.528 ± 0.001	0.767	0.660
	100	1.469 ± 0.005	0.778	0.736

The tracer diffusivities of eucalyptol in liquid ethanol decrease with pressure and increase with temperature (Figure 12) as previously observed for the ternary system eucalyptol/SC-CO_2/ethanol (Figure 9). Nonetheless, these dependencies are not so remarkable owing to the lower compressibility of liquid ethanol and to the considerable volume expansion experienced by the SC-CO_2/ethanol mixture. Regarding the influence of density and the hydrodynamic effect on D_{12} values, for eucalyptol in ethanol (Figures 13 and 14) the trends are similar to those registered for the ternary system (Figures 10 and 11). Again, small deviations from hydrodynamic behavior can be inferred from the non-zero intercept (0.3067×10^{-5} cm^2 s^{-1}) of the linear relationship observed in the D_{12} versus T/μ_1 plot (Figure 14). It is important to emphasize the correlation found between data at the same temperature, which gives rise to sets of three points in Figures 13 and 14.

Finally, the much lower diffusivities of eucalyptol in ethanol than in SC-CO_2/ethanol mixtures are consistent with the results reported by Dong *et al* [75] for L-menthone and L-carvone in mixtures of carbon dioxide and ethanol. A possible explanation for this behavior is the formation of hydrogen bonds between ethanol and the solute molecules, leading to the clustering of solvent molecules around the later, which penalizes the diffusion [84].

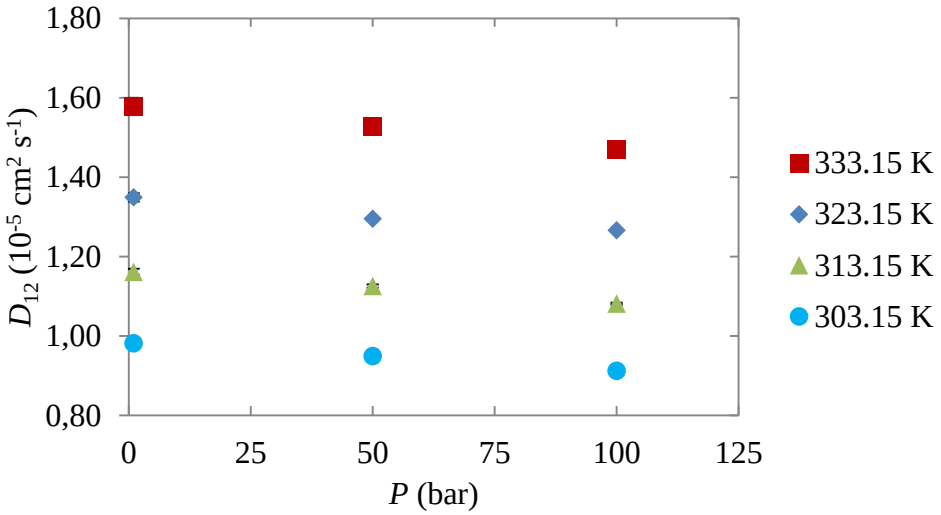

Figure 12 – Tracer diffusion coefficients of eucalyptol in pure liquid ethanol as function of pressure at different temperatures.

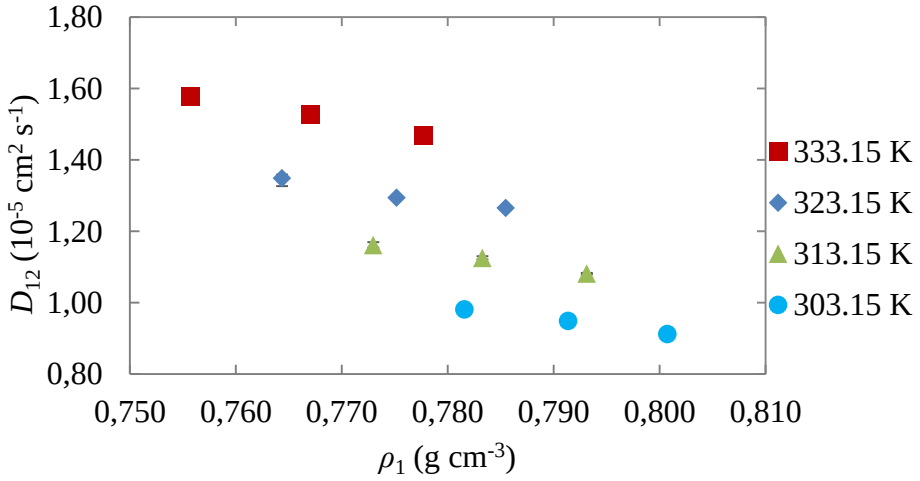

Figure 13 – Tracer diffusion coefficients of eucalyptol in pure liquid ethanol as function of solvent density at different temperatures.

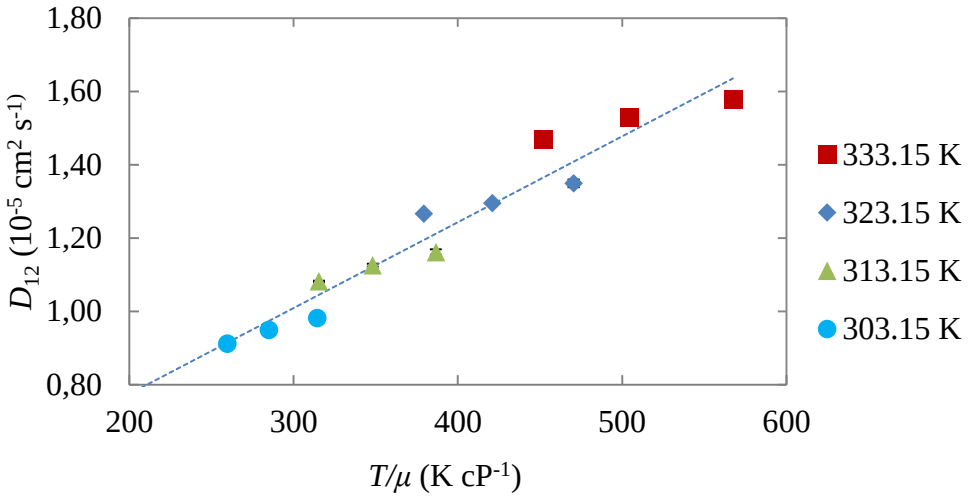

Figure 14 – Tracer diffusion coefficient of eucalyptol in pure liquid ethanol plotted in Stokes-Einstein fashion.

5.4. Modelling eucalyptol tracer diffusion coefficients

Various prediction and correlation models were assessed for modelling the experimental tracer diffusion coefficients of eucalyptol in ethanol and in SC-CO_2/ethanol. Table 3 lists the required physical properties of eucalyptol, CO_2, ethanol and SC-CO_2/ethanol mixture, namely: molecular weight (M_i), acentric factor (ω), critical properties (T_C, P_C and V_C), molar liquid volume (V^*) at reduced temperature (T_r = 0.6), molar volume at normal boiling point estimated by Tyn-Calus method ($V_{TC,bp}$), and the Lennard-Jones diameter (σ_{LJ}) and energy (ε_{LJ}/k_B). The modeling results are summarized in Table 4 and compared to the experimental results in Figure 15.

Table 3 – Physical properties of the pure compounds and SC-CO_2/ethanol mixture studied in this work.

Compound or mixture	M_i g mol^{-1}	ω	T_C K	P_C bar	V_C cm^3 mol^{-1}	V^* cm^3 mol^{-1}	$V_{TC,bp}$ cm^3 mol^{-1}	σ_{LJ} Å	ε_{LJ}/k_b K
CO_2	44.01	0.239 [a]	304.1 [a]	73.8 [a]	93.9 [a]	33.87 [c]	-	3.26192 [f]	500.71 [f]
ethanol	46.069	0.644 [a]	513.9 [a]	61.4 [a]	167.1 [a]	59.36 [c]	-	4.23738 [f]	1291.41 [f]
eucalyptol	154.253	-	695.5 [b]	31.4 [b]	509.5 [b]	-	195.8 [d]	6.18749 [g]	538.32 [g]
CO_2/ethanol [h]	44.174	-	342.28 [e]	89.1 [e]	97.3 [e]	-	-	3.54907 [g]	264.92 [g]

[a] Taken from Reid *et al.* [61]; [b] Estimated by the Joback method [61]; [c] Taken from A. Kreglewski [85]; [d] Estimated by the Tyn and Calus method Eq.84 [61]; [e] T_C estimated by Chueh and Prausnitz [61]; V_C estimated by Chueh and Prausnitz technique later modified by Schick and Prausnitz [61]; P_C estimated by the technique suggested by Kreglewski and Kay [61]; [f] Taken from Liu and Silva [13]; [g] Estimated by Eqs.67-69 [58]; [h] mixture of SC-CO_2 with 8 wt.% ethanol.

Table 4 – Modelling results for D_{12} in ternary and binary systems**.**

			Eucalyptol/SC-CO_2/ethanol		Eucalyptol/ethanol	
Model	Number of Parameters	Eq.	Parameters	AARD (%)	Parameters	AARD (%)
DHB	2	58	V_D = 29.58 cm^3 mol^{-1}; B_{DHB} = 1.415×10^{-7} cm^{-1} mol s^{-1} K$^{-1/2}$	1.60	V_D = 52.15 cm^3·mol^{-1}; B_{DHB} = 9.794×10^{-8} cm^{-1} mol s^{-1} K$^{-1/2}$	7.00
DHB & $V_D(T)$	3	111	(*)	-	B_{DHB} = 2.886×10^{-8} cm^{-1} mol s^{-1} K$^{-1/2}$; $m_{VD} = -0.2413$ cm^3 mol^{-1} K; b_{VD} = 112.41 cm^3 mol^{-1}	3.70
TLSM	0	59 – 66	-	20.49	-	6.75
$TLSM_d$	1	59 – 64, 70 – 71	$k_{12,d} = -1.088\times10^{-1}$	2.58	$k_{12,d} = -3.588\times10^{-2}$	4.76
LSM-MP	0	72 – 81	-	20.48	-	-
LSM-MP-θ_1	1	72 – 81	$\theta_1 = 2.5697$	1.55	-	-

Table 4 (continued)

Model	Number of Parameters	Eq.	Eucalyptol/SC-CO_2/ethanol		Eucalyptol/ethanol	
			Parameters	AARD (%)	Parameters	AARD (%)
Wilke-Chang	0	83 – 85	-	8.00	-	17.67
Lai-Tan	0	86	-	8.36	-	-
mSE_1	0	87 and 88	-	1.34	-	3.84
Vaz *et al.*	0	89	-	1.29		
Magalhães *et al.*	2	90	$a_1 = -0.7763$ $b_1 = -17.08$	1.20	$a_1 = -0.7052$ $b_1 = -17.22$	2.98
	2	91	$a_2 = 6.693\times10^{-6}$ cm^3 cP s^{-1} $b_2 = 5.866\times10^{-6}$ cm^2 s^{-1}	2.21	$a_2 = 8.539\times10^{-6}$ cm^3 cP s^{-1} $b_2 = 1.790\times10^{-6}$ cm^2 s^{-1}	4.22
	2	92	$a_3 = -5.648\times10^{-7}$ cm^5 g^{-1} K^{-1} s^{-1} $b_3 = 6.577\times10^{-7}$ cm^2 K^{-1} s^{-1}	1.69	$a_3 = -3.778\times10^{-7}$ cm^5 g^{-1} K^{-1} s^{-1} $b_3 = -3.326\times10^{-7}$ cm^2 K^{-1} s^{-1}	6.01
	2	93	$a_4 = 4.807\times10^{-8}$ cm^5 g^{-1} K^{-1} s^{-1} $b_4 = 1.905\times10^{-8}$ cm^5 cP^{-1} K^{-1} s^{-1}	1.30	$a_4 = 1.399\times10^{-8}$ cm^5 g^{-1} K^{-1} s^{-1} $b_4 = 2.239\times10^{-8}$ cm^5 cP^{-1} K^{-1} s^{-1}	3.00

(*)The results for the original DHB model are very accurate, with AARD = 1.60 %. Hence, V_D is taken as constant.

In general, very good results were achieved, especially for the ternary system, when using the models of DHB, $TLSM_d$, mSE_1, Vaz *et al.*, and Magalhães *et al.* (AARD = 1.60, 2.58, 1.34, 1.29 and 1.20-2.21 %, respectively). Moreover, for the binary system the modelling results although satisfactory were not so good as for the ternary system. The best results were obtained with the equations of $TLSM_d$, mSE_1, and Magalhães *et al.* (AARD = 4.76, 3.84 and 2.98-6.01 %, respectively). These results can be seen more explicitly in Figure 15, which presents the calculated *versus* experimental D_{12} values for both systems.

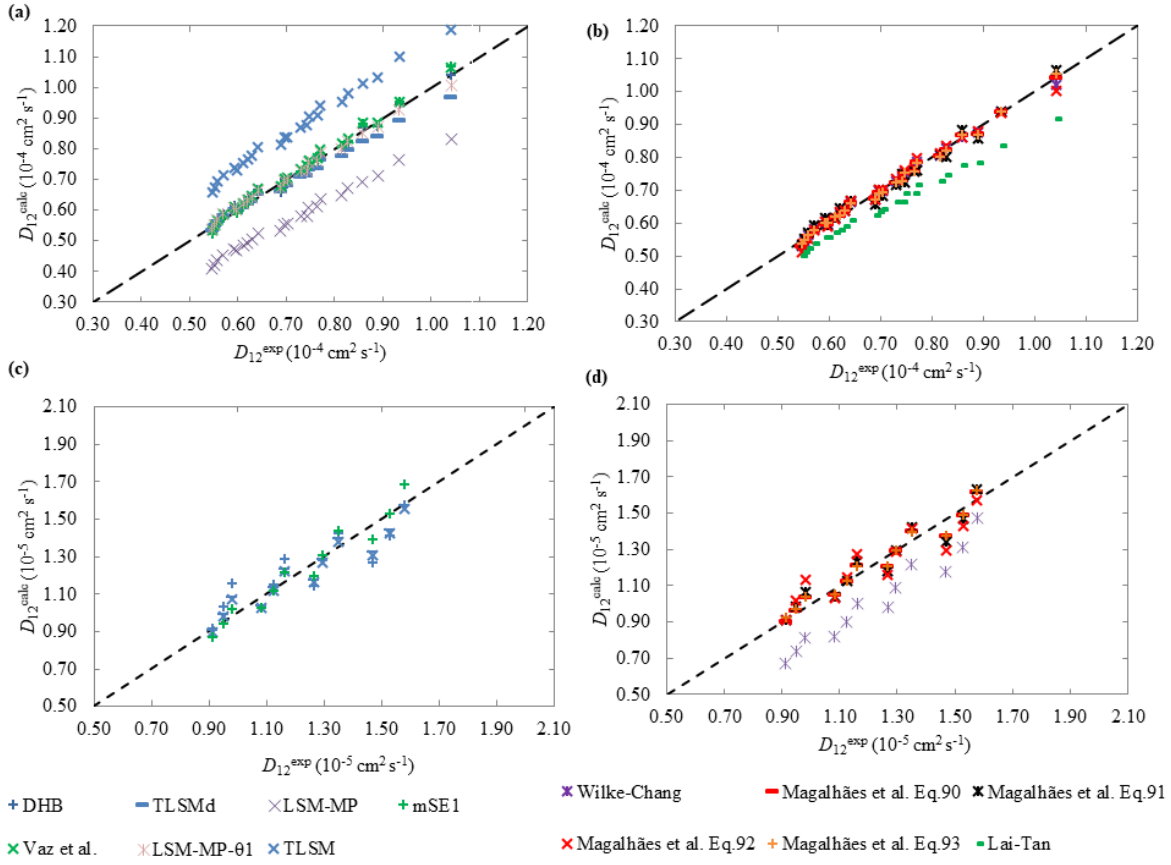

Figure 15 – Experimental *versus* calculated D_{12} values for: (a) & (b) eucalyptol/SC-CO_2/ethanol (8 wt.%), and (c) & (d) eucalyptol/ethanol.

Regarding the hydrodynamic theory based models (Lai-Tan, mSE_1, and Vaz *et al.*) envisaged for the estimation of D_{12} in SC-CO_2, they provided surprisingly good results for the ternary system (eucalyptol/SC-CO_2/ethanol) with AARD as low as 1.29 % (Vaz *et al.*) or 1.34 % (mSE_1). In particular, for the Vaz *et al.* model it is worth mentioning that the input solvent properties were, in this work, the density of pure SC-CO_2 and the viscosity of the SC-CO_2/ethanol mixture. The good results for the predicted diffusion coefficients

(AARD = 1.29 % and maximum error of 4.48 %) clearly show that solvent density is not as crucial as viscosity, mainly for the low ethanol content of this work (8 wt.%). In fact, if the density and viscosity of pure SC-CO_2 were used instead, the AARD would jump to 24.36 %.

The TLSM prediction model estimates the D_{12} values reasonably well for the binary system (AARD = 6.75 %) and not so well (AARD = 20.48 %) for the ternary system (see Figure 15 and Table 4). The overestimation is related to the nature of the model, which was developed for LJ fluids where attractive forces are much weaker than the hydrogen bonds present in both systems. The introduction of one adjustable interaction parameter to the diameter combining rule ($k_{12,d}$ in Eq.70) configures the so-called $TLSM_d$ model, which performed much better (AARDs drop to 4.76 % and 2.58 % for the binary and ternary systems, respectively).

The extension of the TLSM model to multicomponent intradiffusivities of LJ mixtures (LSM-MP) was studied by Merzliak and Pfennig [13,59]. Notwithstanding the final equations (Eqs.72-81) are only applicable to LJ model fluids, this method was tested here for the estimation of D_{12} in the ternary system using two approaches. (i) The LSM-MP model with original published constants (θ_1 = 2.159807, θ_2 = 1.156846, θ_3 = 0.414496, θ_4 = 0.610344, and θ_5 = 0.564022 [13,59]). (ii) The LSM-MP model with distinct constants, hereafter denoted by LSM-MP-θ_1, taking into account the following reasoning. During calculations it was observed that the LSM-MP model is very sensitive to θ_1 which is associated to the LJ diameter (Eqs.74 and 75). Hence, θ_1 was optimized (minimizing AARD) while fixing the remaining four constants equal to those of the Liu-Silva-Macedo model, namely: θ_2 = 1.2588, θ_3 = 0.75 and θ_4 = 0.27862 from Eq.59, and θ_5 = 1/1.3229 = 0.7559 from Eq.62. The newly optimized constant (θ_1 = 2.5697) provides an excellent fitting to the eucalyptol diffusion data (AARD = 1.55 %), as the calculated *versus* experimental D_{12} plot shown in Figure 15.a also demonstrates.

The DHB expression and the four correlations of Magalhães *et al.* achieve good results for both systems, requiring only the knowledge of temperature and the density and viscosity of the solvent. However, for the binary system there is an apparent grouping of the D_{12} values according to the system's temperature (see Figure 15.b) suggesting that the models do not translate well the pressure/temperature effect in this case. Due to its

simplicity, the DHB model will be used to present and discuss a model correction that overcomes this problem.

The minimum molar volume required for diffusion (V_D in Eq.59) exhibits temperature dependent values for a given system (see Figure 16.a) emphasizing the need to express V_D as function of temperature. The same observation was found before in the case of viscosity, i.e. $V_D = V_D(T)$ [13,56]. Assuming a linear dependence for V_D (i.e., $V_D = m_{VD}T + b_{VD}$), the improved DHB model becomes:

$$\frac{D_{12}}{\sqrt{T}} = B_{DHB}[V_m - (m_{VD}T + b_{VD})] \qquad \text{(Eq.111)}$$

where B_{DHB}, m_{VD} and b_{VD} are adjustable parameters obtained by fitting Eq.111 to the experimental (see Figure 16). The optimized parameters were B_{DHB}= 2.886x10^{-8} cm^{-1} mol s^{-1} K$^{-1/2}$, m_{VD}= −0.2413 cm^3 mol^{-1} K and b_{VD}= 112.41 cm^3 mol^{-1}. The graphical representation of D_{12} values calculated with Eq.111 *versus* experimental points is plotted in Figure 16.b, and clearly confirms the elimination of the abovementioned grouping effect. The computed error was very small (AARD = 3.70 %) in contrast to the original 7.00 % found for classical DHB (see Table 4).

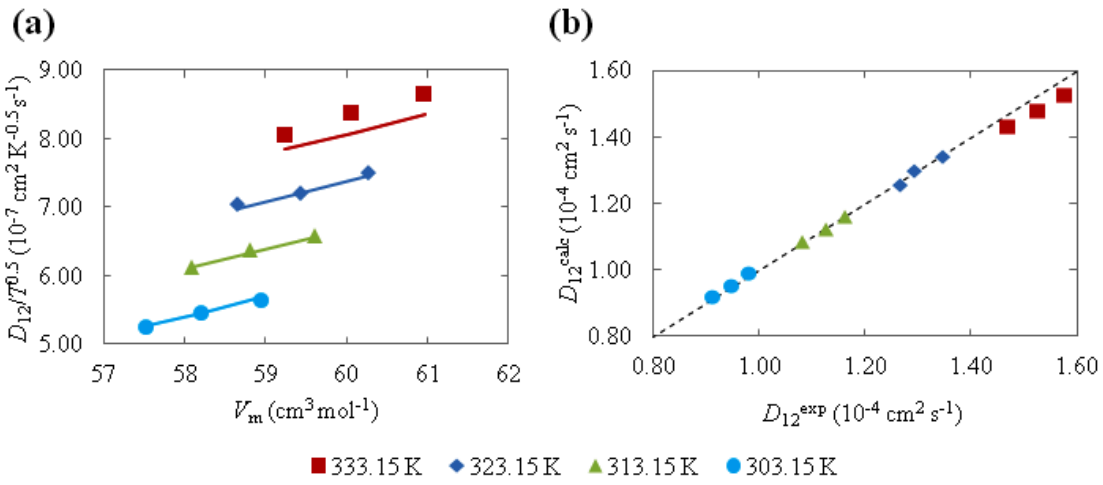

Figure 16 – Experimental and calculated tracer diffusion coefficients of eucalyptol/ethanol system using the modified DHB model given by Eq.111. (a) $D_{12}/T^{0.5}$ values against solvent molar volume; (b) Graphical representation of calculated *versus* experimental D_{12} values. Symbols are data points, full lines are model results.

5.5. Ternary systems database modelling

With the objective to develop accurate D_{12} models for ternary systems (i.e., one solute at infinite dilution in binary solvents), it is necessary to have a large database of experimental data for the validation of the models. During last years, researchers of EgiChem group have been performing this task, collecting 132 ternary liquid and supercritical systems with 1453 data points totally. This database was utilized to test and compare the original LSM-MP model (Eqs. 72-81) and the pseudo-component approach of TLSM model (Eqs. 65-66), which achieved AARDs of 36.08 and 33.45 %, respectively, and demonstrated the poor performance of both predictions. It is worth noting to emphasise that the LSM-MP equations were devised for the intradiffusivities of LJ model mixtures, and that TLSM equations were developed for binary nonpolar or weakly polar systems. Hence, the poor results obtained are not surprising.

In Figures 17 and 18 are plotted the calculated *versus* experimental D_{12} values for both models, where the results for liquid and supercritical systems were plotted using distinct colours (blue-liquid and red-supercritical). One easily confirms that the calculated LSM-MP diffusivities are split into two distinct groups (Figure 18), according to the already mentioned physical state of the solvent. This fact led to the idea of dividing the database into two categories, liquid systems (blue dots) and supercritical systems (red dots), and than re-optimizing the parameters of the model (θ_i) using each part of database. The first group is constituted by 91 systems with 586 experimental points, while the second contains 41 systems with 867 points.

The results obtained for the group of liquid systems attained AARD = 9.39 %, being validated over $0.3937<T^*<1.2458$ and $0.7376<\rho^*<0.9630$, while the group of supercritical systems offered AARD = 9.11 % over $0.5224<T^*<0.7638$ and $0.2654<\rho^*<0.7185$. In comparison to the original errors (36.02 and 34.33 %, respectively) the improvement was extremely significant.

Notwithstanding the low AARDs found in both cases, the group of supercritical points exhibits a large variation of individual AARDs, namely from 2.34 to 40.05 %. This happens since the number of experimental data per system is not uniformly distributed, which means the optimized parameters tend to privilege the largest systems. With respect to the liquids systems, the dispersion was lower, with AARD ranging from 0.30 to 33.95

%. This is clearly shown in Figure 19, which shows the data is unbiasedly distributed along diagonal in both cases, but are more scattered in Figure 19.b for supercritical systems.

The new θ_i values are listed in Table 5, and the properties of the pure components required for the calculations are compiled in Appendix D (Table D.1). The individual results per system that were achieved by the re-optimized TLSM-MP model are compiled in Tables D.2 and D.3.

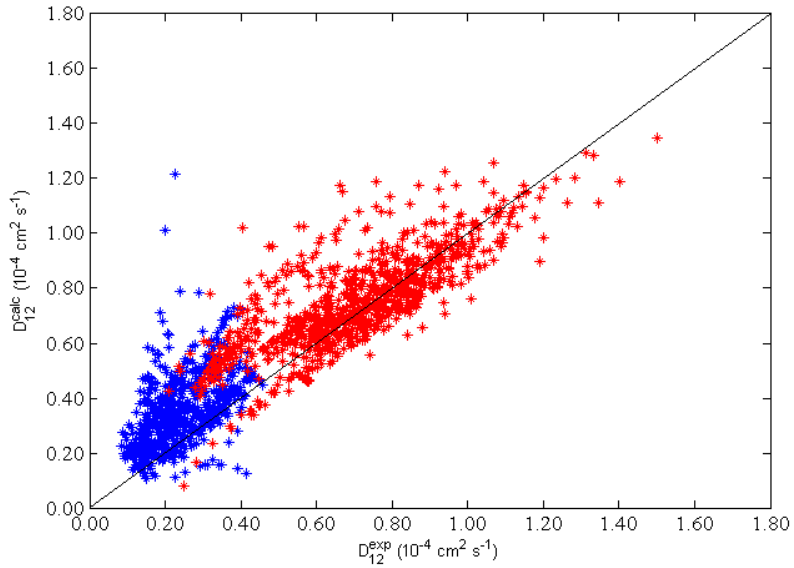

Figure 17 – D_{12} calculated by the TLSM model *versus* experimental D_{12}. Blue dots are liquid systems; red dots are supercritical systems.

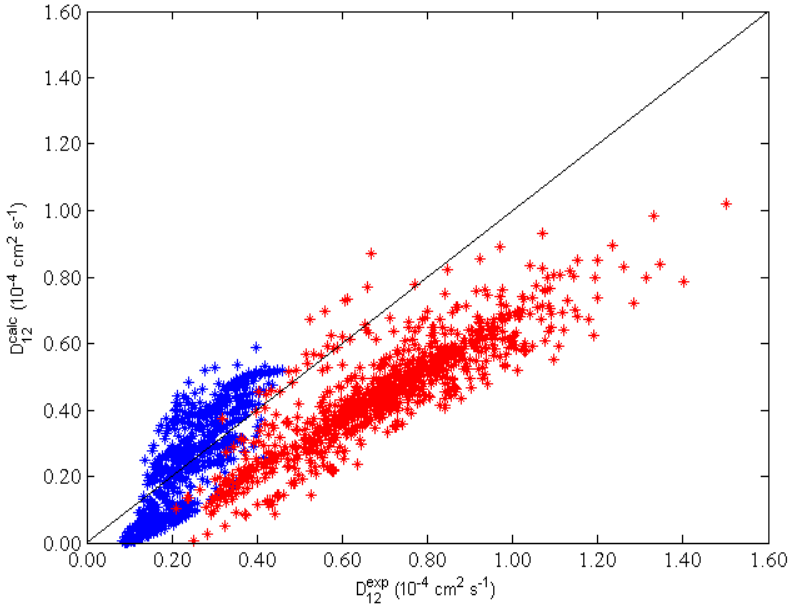

Figure 18 – D_{12} calculated by the LSM-MP model *versus* experimental D_{12}. Blue dots are liquid systems; red dots are supercritical systems.

Table 5 – Optimized constants of the LSM-MP model for liquid and SCF systems.

	Liquid systems	SCF systems
θ_1	3.082	4.32
θ_2	1.198	1.00
θ_3	0.185	0.58
θ_4	0.964	2.39
θ_5	0.380	0.0126

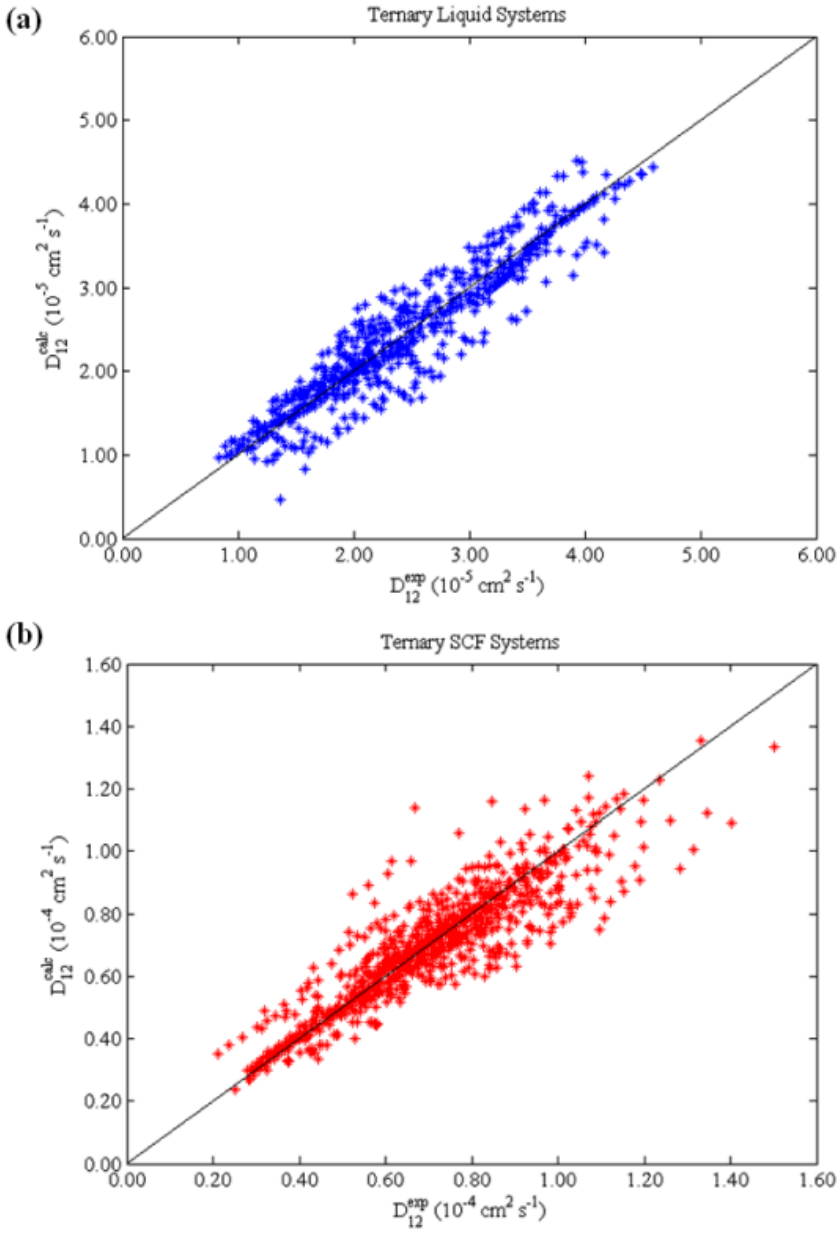

Figure 19 – D_{12} calculated by the corrected LSM-MP model *versus* experimental D_{12}. Results obtained for: **(a)** liquid ternary systems database; **(b)** supercritical ternary systems database.

6. Conclusion and suggestions of future work

In this thesis, the measurement of tracer diffusion coefficients, D_{12}, of eucalyptol in SC-CO_2 modified with ethanol and in liquid ethanol was performed using the CPB method. A wavelength study was carried in order to determine the best conditions to perform the measurements (220 nm for the ternary eucalyptol/ SC-CO_2/ethanol system, and 200 nm for the binary eucalyptol/ethanol system, respectively).

The tracer diffusivities of eucalyptol in SC-CO_2 modified with 8 % (w/w) of ethanol, assessed at temperatures ranging from 303.15 to 333.15 K and pressure between 150 and 275 bar, ranged between 0.547×10^{-4} and 1.042×10^{-4} cm^2 s^{-1}. The diffusion coefficients of eucalyptol in pure liquid ethanol at temperatures ranging between 303.15 and 333.15 K and pressures from 1 to 100 bar were in the range between 0.912×10^{-5} and 1.578×10^{-5} cm^2 s^{-1}. The D_{12} results presented the same trend for both systems and were analyzed in terms of dependency on temperature, pressure, density and Einstein-Stokes coordinates.

A series of models based on free volume and hydrodynamic theories and empirical and semi-empirical correlations were tested and compared to the data experimentally obtained. The Dymon-Hildebrand-Batschinski (DHB) model, the 1-parameter Tracer Liu-Silva-Macedo (TLSMd) model, the modified Stokes-Einstein-1 model, and the Magalhães *et al.* correlations are the ones that present the best results for both systems (AARD = 1.60-7.00, 2.58-4.76, 1.34-3.84 and 1.20-6.01 %, respectively). For the ternary system, it should also be noticed the Wilke-Chang equation (8.00 %), Lai-Tan (8.36 %) and the Vaz *et al.* (1.29 %) predictive models. Regarding the binary system, it should also be highlighted the TLSM model (AARD = 6.75 %) even though it is not theoretically appropriate for the system. Two corrections were suggested, one for the extension of Liu-Silva-Macedo model to multicomponent LJ intradiffusivities using mixing rules of Merzliak and Pfenning (LSM-MP) applied to the ternary system, and one for the DHB model applied to the binary system. In the first case the value of θ_1 was optimized keeping the TLSM values of θ_2 to θ_5 achieving an AARD of 1.55 % (LSM-MP-θ_1). Regarding the DHB model it was suggested that the minimum volume required for diffusion, V_D, should be expressed as a linear function of temperature providing a better performance (AARD = 3.70 %).

Finally the TLSM and LSM-MP models were tested in a D_{12} database constituted by 132 ternary systems with a total of 1453 experimental. The LSM-MP model was the one that showed more promising results therefore a re-optimization of their constants was

proposed. By splitting the database into two categories, namely liquid and supercritical systems, new θ values were determined for each group. The AARD obtained for liquid was 9.39 % and for supercritical 9.11 %. It should be noted that for supercritical systems the range of AARD for individual systems is very large thus the model is not reliable.

Suggestions of future work

Regarding future work, considering there is still a great lack of experimental data for D_{12} in SC-CO_2, especially when it is modified with a cosolvent, it would be of great importance to: measure D_{12} values of other bioactive compounds at various conditions; continue the development of accurate predictive model to estimate D_{12} in multicomponent systems; evaluate the reliability of the changes presently suggested for the LSM-MP model.

References

[1] C.A.. Afonso, J.G. Crespo, Green Separation Processes: Fundamental and Applications, Wiley-VCH, 2005.

[2] M.J.H. Akanda, M.Z.I. Sarker, S. Ferdosh, M.Y.A. Manap, N.N.N. Ab Rahman, M.O. Ab Kadir, Applications of Supercritical Fluid Extraction (SFE) of Palm Oil and Oil from Natural Sources, Molecules. 17 (2012) 1764–1794.

[3] P.E. Savage, S. Gopalan, T.I. Mizan, C.J. Martino, E.E. Brock, Reactions at supercritical conditions: Applications and fundamentals, AIChE J. 41 (1995) 1723–1778.

[4] E.L.G. Oliveira, A.J.D. Silvestre, C.M. Silva, Review of kinetic models for supercritical fluid extraction, Chem. Eng. Res. Des. 89 (2011) 1104–1117.

[5] G. Brunner, Applications of Supercritical Fluids, Annu. Rev. Chem. Biomol. Eng. 1 (2010) 321–342.

[6] M. Herrero, J.A. Mendiola, A. Cifuentes, E. Ibáñez, Supercritical fluid extraction: Recent advances and applications, J. Chromatogr. A. 1217 (2010) 2495–2511.

[7] G. Guiochon, A. Tarafder, Fundamental challenges and opportunities for preparative supercritical fluid chromatography, J. Chromatogr. A. 1218 (2011) 1037–1114.

[8] I. Medina, Determination of diffusion coefficients for supercritical fluids, J. Chromatogr. A. 1250 (2012) 124–140.

[9] M. Melo, R. Domingues, A. Silvestre, C. Silva, Extraction and Purification of Triterpenoids using Supercritical Fluids: From Lab to Exploitation, Mini. Rev. Org. Chem. 11 (2014) 362–381.

[10] M.M.R. De Melo, A.J.D. Silvestre, C.M. Silva, Supercritical fluid extraction of vegetable matrices: Applications, trends and future perspectives of a convincing green technology, J. Supercrit. Fluids. 92 (2014) 115–176.

[11] M.M.R. de Melo, H.M.A. Barbosa, C.P. Passos, C.M. Silva, Supercritical fluid extraction of spent coffee grounds: Measurement of extraction curves, oil characterization and economic analysis, J. Supercrit. Fluids. 86 (2014) 150–159.

[12] R.B. Gupta, J.-J. Shim, Solubility in Supercritical Carbon Dioxide, CRC Press, NW, 2007.

[13] H. Liu, C.M. Silva, Modelling of Transport Properties of Hard Sphere Fluids and Related Systems and its Applications, in: Lect. Notes Phys. 753 Theory Simul.

Hard-Sph. Fluids Relat. Syst., 2008: pp. 37–109.

[14] J.D. Seader, W.D. Seider, D.R. Lewin, L. Boulle, A. Rycrof, Separation Process Principles Chemical and Biochemical Operations, third, Wiley, USA, 2006.

[15] E.L. Cussler, Diffusion Mass Transfer in Fluid Systems, Third ed., Cambridge University Press, NY, USA, 1997.

[16] D.D. Do, Adsorption Analysis: Equilibria and Kinetics, Imperial College Press, London, 1998.

[17] J. Cordeiro, A.L. Magalhães, A.A. Valente, C.M. Silva, Experimental and theoretical analysis of the diffusion behavior of chromium(III) acetylacetonate in supercritical CO2, J. Supercrit. Fluids. 118 (2016) 153–162.

[18] R. V. Vaz, A.L. Magalhães, C.M. Silva, Improved Stokes-Einstein based models for diffusivities in supercritical CO2, J. Taiwan Inst. Chem. Eng. 45 (2014) 1280–1284.

[19] M. Eggersdorfer, Terpenes, in: ULLMANN'S, Sixth ed., Ludwigs, 2002.

[20] C.H. Bibb, Method of separating cineols from hydrocarbons of similar boiling range, 1937.

[21] A.I. Caceres, B. Liu, S. V Jabba, S. Achanta, J.B. Morris, S.-E. Jordt, Transient Receptor Potential Cation Channel Subfamily M Member 8 channels mediate the anti-inflammatory effects of eucalyptol, Br. J. Pharmacol. 174 (2017) 867–879.

[22] R. Moghimi, A. Aliahmadi, H. Rafati, Ultrasonic nanoemulsification of food grade trans-cinnamaldehyde: 1,8-Cineol and investigation of the mechanism of antibacterial activity, Ultrason. Sonochem. 35 (2017) 415–421.

[23] M. Soh, G.W. Stachowiak, The application of cineole as a grease solvent, Flavour Fragr. J. 17 (2002) 278–286.

[24] K.K. Liong, P.A. Wells, N.R. Foster, Diffusion in supercritical fluids, J. Supercrit. Fluids. 4 (1991) 91–108.

[25] G. Taylor, Dispersion of soluble matter in solvent flowing slowly through a tube, Proc. Phys. Soc. Sect. B. (1953).

[26] G. Taylor, Diffusion and Mass Transport in Tubes, Proc. Phys. Soc. Sect. B. 67 (1954) 857–869.

[27] G. Taylor, The Dispersion of Matter in Turbulent Flow through a Pipe, Proc. R. Soc. London A Math. Phys. Eng. Sci. 223 (1954).

[28] R. Aris, On the dispersion of a solute by diffusion, convection and exchange

between phases, Soc. R. 252 (1959) 538–550.

[29] J.C. Giddings, S.L. Seager, Rapid Determination of Gaseous Diffusion Coefficients by Means of a Gas Chromatography Apparatus, J. Chem. Phys. 33 (1960) 1579.

[30] Z. Balenovic, M.N. Myers, J.C. Giddings, Binary Diffusion in Dense Gases to 1360 atm by the Chromatographic Peak- Broadening Method, J. Chem. Phys. 52 (1970) 915.

[31] A.C. Ouano, Diffusion in Liquid Systems. 1. A Simple and Fast Method of Measuring Diffusion Constants, Ind. Eng. Chem. Fundam. 11 (1972) 268.

[32] R. Feist, G.M. Schneider, Determination of Binary Diffusion Coefficients of Benzene, Phenol, Naphthalene and Caffeine in Supercritical CO2 between 308 and 333K in the Pressure Range 80 to 160 bar with Supercritical Fluid Chromatography (SFC)., Sep. Sci. Technol. 17 (1982) 261.

[33] R. V. Vaz, A.L. Magalhães, A.A. Valente, C.M. Silva, Measurement and modeling of tracer diffusivities of α-pinene in supercritical CO2, and analysis of their hydrodynamic and free-volume behaviors, J. Supercrit. Fluids. 107 (2016) 690–698.

[34] J. Cordeiro, A.L. Magalhães, A.A. Valente, C.M. Silva, Experimental and theoretical analysis of the diffusion behavior of chromium(III) acetylacetonate in supercritical CO2, J. Supercrit. Fluids. 118 (2016) 153–162.

[35] T. Funazukuri, C.Y. Kong, S. Kagei, Impulse response techniques to measure binary diffusion coefficients under supercritical conditions, J. Chromatogr. A. 1037 (2004) 411–429.

[36] C.Y. Kong, T. Funazukuri, S. Kagei, Chromatographic impulse response technique with curve fitting to measure binary diffusion coefficients and retention factors using polymer-coated capillary columns, J. Chromatogr. A. 1035 (2004) 177–193.

[37] R.J. Nunge, T.-S. Lin, W.N. Gill, Laminar dispersion in curved tubes and channels, J. Fluid Mech. 51 (1972) 363.

[38] J.M.H. Levelt Sengers, U.K. Deiters, U. Klask, P. Swidersky, G.M. Schneider, Application of the Taylor dispersion method in supercritical fluids, Int. J. Thermophys. 14 (1993) 893–922.

[39] C.M. Silva, Coeficientes de Difusão em Misturas Supercríticas, FEUP, 1998.

[40] E.T. van der Laan, Notes on the diffusion type model for longitudinal mixing in flow, Chem. Eng. Sci. 7 (1958) 187–191.

[41] J.A. Moulijn, R. Spijker, J.F.M. Kolk, Axial dispersion of gases flowing through coiled columns, J. Chromatogr. A. 142 (1977) 155–166.

[42] A. Alizadeh, C.A. Nieto de Castro, W.A. Wakeham, The theory of the Taylor dispersion technique for liquid diffusivity measurements, Int. J. Thermophys. 1 (1980) 243–284.

[43] S.R. Springston, M. Novotny, Coiling-induced secondary flow in capillary supercritical fluid chromatography, Anal. Chem. 58 (1986) 2699–2704.

[44] C.Y. Kong, T. Funazukuri, S. Kagei, G. Wang, F. Lu, T. Sako, Applications of the chromatographic impulse response method in supercritical fluid chromatography, J. Chromatogr. A. 1250 (2012) 141–156.

[45] O. Levenspiel, W.K. Smith, Notes on the diffusion-type model for the longitudinal mixing of fluids in flow, Chem. Eng. Sci. 50 (1995) 3891–3896.

[46] J.C. Giddings, S.L. Seager, Method for rapid determination of diffusion coefficients, Ind. Eng. Chem. Fundam. 1 (1962) 277–283.

[47] G. Madras, B.L. Hamilton, M. a. Matthews, Influence of adsorption on the measurement of diffusion coefficients by Taylor dispersion, Int. J. Thermophys. 17 (1996) 373–389.

[48] C. Lait, C. Tan, Measurement of Molecular Diffusion Coefficients in Supercritical Carbon Dioxide Using a Coated Capillary Column, Ind. Eng. Chem. Res. 34 (1995) 674–680.

[49] W.A. Wakeham, A. Nagashima, J. V. Sengers, eds., Measurement of the Transport Properties of Fluids - Experimental Thermodynamics Volume III, Blackwell Scientific Publications, 1991.

[50] T. Funazukuri, C.Y. Kong, S. Kagei, Infinite-Dilution Binary Diffusion Coefficients of 2-Propanone, 2-Butanone, 2-Pentanone, and 3-Pentanone in CO2 by the Taylor Dispersion Technique from 308.15 to 328.15 K in the Pressure Range from 8 to 35 MPa, Int. J. Thermophys. 21 (2000) 1279–1290.

[51] C.M. Silva, C.A. Filho, M.B. Quadri, E.A. Macedo, Binary diffusion coefficients of α-pinene and β-pinene in supercritical carbon dioxide, J. Supercrit. Fluids. 32 (2004) 167–175.

[52] N. Wakao, S. Kaguei, Heat and Mass Transfer in Packed Beds, 1982.

[53] R. Aris, On the dispersion of a solute in a fluid flowing through a tube, Soc. R.

(1956).

[54] T. Funazukuri, C.Y. Kong, S. Kagei, Measurements of binary diffusion coefficients for some low volatile compounds in supercritical carbon dioxide by input–output response technique with two diffusion columns connected in series, Fluid Phase Equilib. 194 (2002) 1169–1178.

[55] J.H. Dymond, Corrected Enskog theory and transport coefficients of liquids, J. Chem. Phys. 60 (1974) 969–973.

[56] J. Millat, J.H. Dymond, C.A. Nieto de Castro, eds., Transport Properties of Fluids. Their correlation, prediction and estimation., Cambridge University Press, Cambridge, 1996.

[57] H. Liu, C.M. Silva, E.A. Macedo, New Equations for Tracer Diffusion Coefficients of Solutes in Supercritical and Liquid Solvents Based on the Lennard-Jones Fluid Model, Ind. Eng. Chem. Res. 36 (1997) 246–252.

[58] A.L. Magalhães, S.P. Cardoso, B.R. Figueiredo, F.A. Da Silva, C.M. Silva, Revisiting the liu-silva-macedo model for tracer diffusion coefficients of supercritical, liquid, and gaseous systems, Ind. Eng. Chem. Res. 49 (2010) 7697–7700.

[59] T. Merzliak, A. Pfennig, Development of a model for the Description of Intra-diffusion in Homogeneous Liquid Lennard–Jones Mixtures, Mol. Simul. 30 (2004) 459–468.

[60] C.R. Wilke, P. Chang, Correlation of diffusion coefficients in dilute solutions, A.I.Ch.E. J. (1955) 264–270.

[61] R.C. Reid, J.M. Prausnitz, B.E. Poling, The properties of Gases & Liquids, Fifth ed., McGraw-Hill International Editions, New York, 2001.

[62] A.L. Magalhães, R. V. Vaz, R.M.G. Gonçalves, F.A. Da Silva, C.M. Silva, Accurate hydrodynamic models for the prediction of tracer diffusivities in supercritical carbon dioxide, J. Supercrit. Fluids. 83 (2013) 15–27.

[63] R. V. Vaz, A.L. Magalhães, C.M. Silva, Prediction of binary diffusion coefficients in supercritical CO2 with improved behavior near the critical point, J. Supercrit. Fluids. 91 (2014) 24–36.

[64] A.L. Magalhães, P.F. Lito, F.A. Da Silva, C.M. Silva, Simple and accurate correlations for diffusion coefficients of solutes in liquids and supercritical fluids

over wide ranges of temperature and density, J. Supercrit. Fluids. 76 (2013) 94–114.

[65] P.F. Lito, A.L. Magalhães, J.R.B. Gomes, C.M. Silva, Universal model for accurate calculation of tracer diffusion coefficients in gas, liquid and supercritical systems, J. Chromatogr. A. 1290 (2013) 1–26.

[66] H. Liu, C.M. Silva, E.A. Macedo, Unified approach to the self-diffusion coefficients of dense fluids over wide ranges of temperature and pressure - Hard-sphere, square-well, Lennard-Jones and real substances, Chem. Eng. Sci. 53 (1998) 2403–2422.

[67] J. Leite, Difusividades de compostos bioativos em CO2 supercrítico, Aveiro, 2016.

[68] M.J. Assael, J.H. Dymond, S.K. Polimatidou, Correlation and prediction of dense fluid transport coefficients, Fluid Phase Equilib. 15 (1994) 189–201.

[69] J.J. Cano-Gómez, G.A. Iglesias-Silva, V. Rico-Ram-erez, M. Ramos-Estrada, K.R. Hall, A new correlation for the prediction of refractive index and liquid densities of 1-alcohols, Fluid Phase Equilib. 387 (2015) 117–120.

[70] J.J. Cano-Gómez, G.A. Iglesias-Silva, M. Ramos-Estrada, Correlations for the prediction of the density and viscosity of 1-alcohols at high pressures, Fluid Phase Equilib. 404 (2015) 109–117.

[71] C.L. Yaws, X. Lin, L. Bu, D.R. Balundgi, S. Tripathi, Chemical Properties Handbook: Physical, Thermodynamic, Environmental, Transport, Safety, and Health Related Properties for Organic and Inorganic Chemical, McGraw-Hill, Beaumont, Texas, 1999.

[72] M. Kariznovi, H. Nourozieh, J. Abedi, Experimental measurements and predictions of density, viscosity, and carbon dioxide solubility in methanol, ethanol, and 1-propanol, J. Chem. Thermodyn. 57 (2013) 408–415.

[73] J. Kendall, K.P. Monroe, The Viscosity of Liquids. II. The Viscosity-Composition Curve for Ideal Liquid Mixtures. 1, J. Am. Chem. Soc. 39 (1917) 1787–1802.

[74] V. V. Altunin, M.. Skhabetinov, Viscosity of liquid and gaseous carbon dioxide at temperatures 220−1300 K and pressure up to 1200 bar, Teploenergetika. 8 (1972) 85–89.

[75] X. Dong, B. Su, H. Xing, Y. Yang, Q. Ren, Diffusion coefficients of l-menthone and l-carvone in mixtures of carbon dioxide and ethanol, J. Supercrit. Fluids. 55 (2010) 86–95.

[76] X. Dong, B. Su, H. Xing, Z. Bao, Y. Yang, Q. Ren, Cosolvent effects on the

diffusions of 1,3-dichlorobenzene, l-carvone, geraniol and 3-fluorophenol in supercritical carbon dioxide, J. Supercrit. Fluids. 58 (2011) 216–225.

[77] C.M. Silva, H. Liu, E.A. Macedo, Models for self-diffusion coefficients of dense fluids, including hydrogen-bonding substances, Chem. Eng. Sci. 53 (1998) 2423–2429.

[78] H. Liu, C.M. Silva, E.A. Macedo, Generalised free-volume theory for transport properties and new trends about the relationship between free volume and equations of state, Fluid Phase Equilib. 202 (2002) 89–107.

[79] T. Wells, N.R. Foster, R.P. Chaplin, Diffusion of Phenylacetic Acid and Vanillin in Supercritical Carbon Dioxide, Ind. Eng. Chem. Res. 31 (1992) 927–934.

[80] Y. Yang, H. Yan, B. Su, H. Xing, Z. Bao, Z. Zhang, X. Dong, Q. Ren, Diffusion coefficients of C18 unsaturated fatty acid methyl esters in supercritical carbon dioxide containing 10% mole fraction ethanol as modifier, J. Supercrit. Fluids. 83 (2013) 146–152.

[81] T. Funazukuri, T. Sugihara, K. Yui, T. Ishii, M. Taguchi, Measurement of infinite dilution diffusion coefficients of Vitamin K3 in CO2 expanded methanol, J. Supercrit. Fluids. 108 (2016) 19–25.

[82] C. Pizarro, O. Suárez-Iglesias, I. Medina, J.L. Bueno, Binary diffusion coefficients for 2,3-dimethylaniline, 2,6-dimethylaniline, 2-methylanisole, 4-methylanisole and 3-nitrotoluene in supercritical carbon dioxide, J. Supercrit. Fluids. 48 (2009) 1–8.

[83] C.M. Silva, E.A. Macedo, Diffusion coefficients of ethers in supercritical carbon dioxide, Ind. Eng. Chem. Res. 37 (1998) 1490–1498.

[84] E.L. Cussler, Cluster diffusion in liquids, AIChE J. 26 (1980) 43–51.

[85] A. Kreglewski, Second virial coefficient of real gases, J. Phys. Chem. 73 (1969) 608–615.

[86] A.L. Magalhães, F.A. Da Silva, C.M. Silva, New tracer diffusion correlation for real systems over wide ranges of temperature and density, Chem. Eng. J. 166 (2011) 49–72.

[87] C. Mantell, M. Rodríguez, E. Martínez De La Ossa, Estimation of the diffusion coefficient of a model food dye (malvidin 3,5-diglucoside) in a high pressure CO2 + methanol system, J. Supercrit. Fluids. 29 (2004) 165–173.

[88] D.H. Chen, M. V. Dinivahi, C.-Y. Jeng, New Acentric Factor Correlation Based on

the Antoine Equation, Ind. Eng. Chem. Res. 32 (1993) 241–244.

[89] Aspen Plus: Getting Started building and Running a Process Model, Version Number: 8.4, Aspen Technology, Inc., Burlington, MA, USA, 2013.

Appendix A – Compounds and properties

In this section the chemical compounds used in this work are presented along side with the corresponding properties.

Ethanol

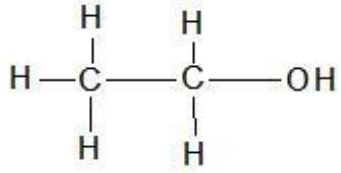

Figure A. 1 – Ethanol molecular structure

CAS: 64-17-5

Chemical formula: C_2H_5OH

Supplier: Fisher Chemical

Molecular weight: 46.069 g·mol^{-1}

Carbon dioxide

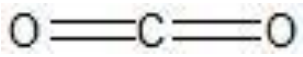

Figure A. 2 – Carbon dioxide molecular structure

CAS: 124-38-9

Chemical formula: CO_2

Supplier: Praxair

Purity: 99.999% (v/v)

Molecular weight: 44.010 g·mol^{-1}

Eucalyptol

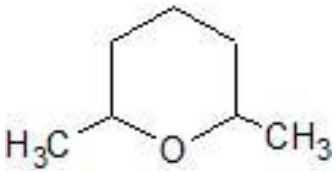

Figure A. 3 – Eucalyptol molecular structure

CAS: 470-82-6

Chemical formula: $C_{10}H_{18}O$

Supplier: José M. Vaz Pereira, LTD

Purity: 100 %

Molecular weight: 154.253 g·mol^{-1}

Appendix B – Critical properties estimation.

For estimation of the critical temperature of the mixture SC-CO2/ethanol, T_{cT} the method of Chueh Prausnitz was used. The method it is described as follows:

$$T_{cT} = \sum_j \theta_j T_{cj} + \sum_i \sum_j \theta_j \theta_i \tau_{ij} \quad \text{(Eq.D.1)}$$

where θ_j is the surface fraction calculated by:

$$\theta_j = \frac{y_j V_{cj}^{2/3}}{\sum_i y_i V_{ci}^{2/3}} \quad \text{(Eq.D.2)}$$

and τ_{ij} is an interaction parameter calculated by the following set of equations:

$$\psi_T = A + B\delta_T + C\delta_T^2 + D\delta_T^3 + E\delta_T^4 \quad \text{(Eq.D.3)}$$

$$\psi_T = \frac{2\tau_{ij}}{T_{ci} + T_{cj}} \quad \text{(Eq.D.4)}$$

$$\delta_{\mathrm{T}} = \left|\frac{T_{\mathrm{i}} - T_{\mathrm{cj}}}{T_{\mathrm{ci}} + T_{\mathrm{cj}}}\right| \quad \text{(Eq.D.5)}$$

where A=-0.0953; B =2.185; C =-33.985; D =179.068; E =-264.522.

For the estimation of the mixture's critical volume, V_{CT}, the method proposed by Chueh and Prausnitz later modified by Schick and Prausnitz was used. The method is described as follows:

$$V_{\mathrm{cT}} = \sum_{\mathrm{j}} \theta_{\mathrm{j}} V_{\mathrm{Cj}} + \sum_{\mathrm{i}} \sum_{\mathrm{j}} \theta_{\mathrm{j}} \theta_{\mathrm{i}} \upsilon_{\mathrm{ij}} \quad \text{(Eq.D.6)}$$

θ_{j} is calculated by Eq.D.2 and υ_{ij} is calculated by the following equations:

$$\psi_{\upsilon} = A + B\delta_{\upsilon} + C\delta_{\upsilon}^2 + D\delta_{\upsilon}^3 + E\delta_{\upsilon}^4 \quad \text{(Eq.D.7)}$$

$$\psi_{\upsilon} = \frac{2\upsilon_{\mathrm{ij}}}{V_{\mathrm{cj}} + V_{\mathrm{ci}}} \quad \text{(Eq.D.8)}$$

$$\delta_{\upsilon} = \left|\frac{V_{\mathrm{ci}}^{2/3} - V_{\mathrm{cj}}^{2/3}}{V_{\mathrm{ci}}^{2/3} + V_{\mathrm{cj}}^{2/3}}\right| \quad \text{(Eq.D.9)}$$

where A = -0.4957; B = 17.1185; C = -168.56; D = 587.05; E = -698.89.

Finally for the estimation of the critical pressure,P_{CT} , of the mixture the Kreglewski and Kay method was used:

$$V_{12}^{*1/3} = \frac{\left[V_1^{*1/3} + V_2^{*1/3}\right]^3}{8} \quad \text{(Eq.D.10)}$$

$$V^* = V_1^* y_1 + V_2^* y_2 + \left(2V_{12}^{*1/3} - V_1^* - V_2^*\right) y_1 y_2 \quad \text{(Eq.D.11)}$$

$$\theta_1 = \frac{y_1 V_{\mathrm{C1}}^{*1/3}}{y_1 V_{\mathrm{C1}}^{*1/3} + y_2 V_{\mathrm{C2}}^{*1/3}} \quad \text{(Eq.D.12)}$$

$$\theta_2 = 1 - \theta_1 \quad \text{(Eq.D.13)}$$

$$T_{12}^* = \frac{2V_{12}^{*1/3}}{V_1^{*1/3}/T_{\mathrm{C1}} + V_2^{*1/3}/T_{\mathrm{C2}}} \quad \text{(Eq.D.14)}$$

$$T^* = V^{*1/3}\left[\frac{T_{\mathrm{C1}}\theta_1}{V_1^{*1/3}} + \frac{T_{\mathrm{C2}}\theta_2}{V_2^{*1/3}} + \left(\frac{2T_{12}^*}{V_{12}^{*1/3}} - \frac{T_{\mathrm{C1}}}{V_1^{*1/3}} - \frac{T_{\mathrm{C2}}}{V_2^{*1/3}}\right)\theta_1\theta_2\right] \quad \text{(Eq.D.15)}$$

$$\omega_{12} = \frac{2}{1/\omega_1 + 1/\omega_2} \quad \text{(Eq.D.16)}$$

$$\omega = \omega_1\theta_1 + \omega_2\theta_2 + (2\omega_{12} - \omega_1 - \omega_2)\theta_1\theta_2 \quad \text{(Eq.D.17)}$$

$$\mathrm{P}^* = \frac{T^*}{V^{*1/3}} \frac{P_{\mathrm{c1}}\theta_1 + P_{\mathrm{c2}}\theta_2}{\frac{T_{\mathrm{c1}}\theta_1}{V_1^{*1/3}} + \frac{T_{\mathrm{c2}}\theta_2}{V_2^{*1/3}}} \quad \text{(Eq.D.18)}$$

$$P_{\mathrm{cT}} = P^*\left[1 + (5.808 + 4.93\omega)\left(\frac{T_{\mathrm{cT}}}{T^*} - 1\right)\right] \quad \text{(Eq.D.19)}$$

It is recommended that T_{CT} should be calculated by:

$$T_{\mathrm{cT}} = \sum_{\mathrm{j}} \frac{y_{\mathrm{j}} V_{\mathrm{cj}}}{\sum_{\mathrm{i}} y_{\mathrm{i}} V_{\mathrm{ci}}} T_{\mathrm{cj}} \quad \text{(Eq.D.20)}$$

Appendix C – Eucalyptol spectrum

In Figure C.1 can be observed the eucalyptol spectrum from 190 to 390 nm.

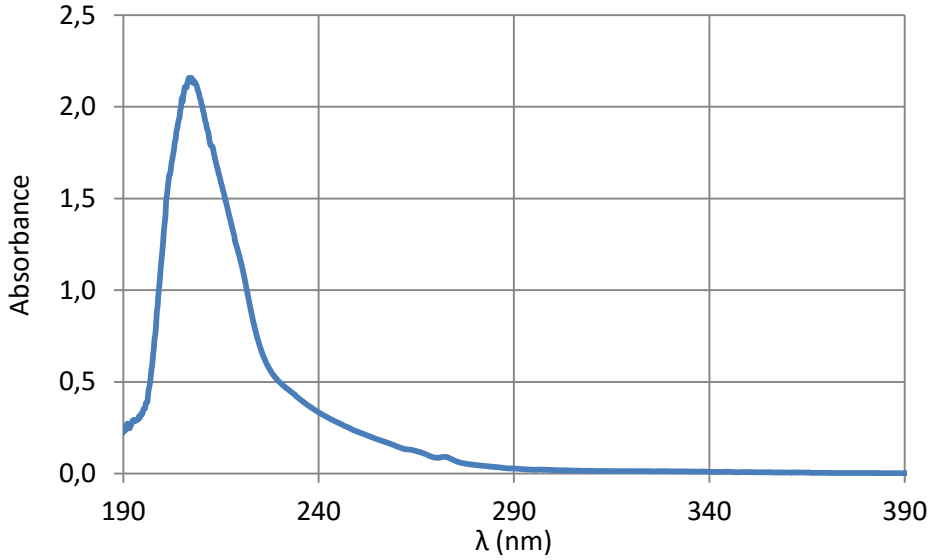

Figure C. 1 – Eucalyptol spectrum ranging from 190 to 390 nm.

Appendix D – Ternary systems database results and compound properties

Table D. 1 – Compounds properties used in the TLSM and TLSM-MP models

Compound name	Cas Number	Formula	M_i g mol^{-1}	ω	T_c K	P_c bar	V_c cm^3 mol^{-1}	V^* cm^3 mol^{-1}	σ_{LJ} Å	ε_{LJ}/k_b K
1,2-dichlorobenzene	135-01-3	$C_6H_4Cl_2$	147.004	0.272 [a]	729.00 [b]	41.00 [b]	360.00 [b]	-	5.79009 [b]	564.25 [b]
1,3-dichlorobenzene	541-73-1	$C_6H_4Cl_2$	147.004	0.272 [a]	693.14 [a]	39.86 [a]	361.5 [a]	-	5.75091 [i]	564.48 [i]
1,4-dioxane	123-91-1	$C_4H_8O_2$	88.106	0.278 [g]	587.00 [a]	51.70 [a]	238.00 [a]	91.20 [f]	5.03437 [b]	454.34 [b]
2-nitroanisole	91-23-6	$C_7H_7NO_3$	153.14	0.559 [g]	782.00 [b]	37.60 [b]	422.00 [b]	-	6.07271 [b]	605.27 [b]
2-phenylethyl acetate	103-45-5	$C_{10}H_{12}O_2$	164.2	0.777 [l]	712.23 [b]	30.12 [b]	524.15 [b]	-	6.31046 [b]	551.27 [b]
3-fluorophenol	372-20-3	FC_6H_4OH	112.1	0.581 [l]	663.74 [h]	53.61 [h]	250.00 [h]	-	5.17387 [i]	513.73 [i]
3-phenylpropyl acetate	122-72-5	$C_{11}H_{14}O_2$	178.231	0.599 [l]	718.70 [a]	27.23 [a]	580.37 [a]	-	6.51801 [b]	556.27 [b]
acetone	666-52-4	C_3H_6O	58.08	0.307 [a]	508.10 [b]	47.00 [b]	209.00 [b]	74.71 [f]	4.67012 [b]	332.97 [b]
acetonitrile	75-05-8	C_2H_3N	41.05	0.331 [g]	545.50 [b]	48.30 [b]	173.00 [b]	55.00 [f]	4.02424 [b]	652.53 [b]
acridine	260-94-6	$C_{13}H_9N$	179.22	0.439 [g]	905.00 [h]	36.40 [h]	619.15 [h]	-	6.40475 [b]	700.47 [b]
benzene	71-43-2	C_6H_6	78.11	0.210 [a]	562.20 [b]	48.90 [b]	259.00 [b]	93.97 [f]	5.19165 [b]	308.43 [b]
benzoic acid	65-85-0	$C_7H_6O_2$	122.124	0.620 [a]	752.00 [a]	45.60 [a]	341.00 [a]	-	5.65763 [b]	582.05 [b]
benzonitrile	100-47-0	C_6H_5CN	103.124	0.342 [g]	699.40 [h]	42.20 [h]	345.50 [h]	-	5.66632 [i]	541.34 [i]
benzyl acetate	140-11-4	$C_9H_{10}O_2$	150.17	0.474 [g]	699.00 [a]	31.80 [a]	449.00 [a]	-	6.17454 [b]	541.03 [b]
carbon dioxide	124-38-9	CO_2	44.01	0.225 [a]	304.10 [a]	73.80 [a]	93.90 [a]	33.87 [f]	3.26192 [b]	500.71 [b]
carbon tetrachloride	56-23-5	CCl_4	153.82	0.191[g]	556.40 [b]	45.60 [b]	275.90 [b]	101.60 [f]	5.29240 [b]	418.84 [b]
chlorobenzene	108-90-7	C_6H_5Cl	112.56	0.325 [a]	632.40 [b]	45.20 [b]	308.00 [b]	-	5.56838 [b]	207.50 [b]
cyclohexane	110-82-7	C_6H_{12}	84.162	0.211 [a]	553.50 [a]	40.73 [a]	308.00 [a]	113.50[f]	5.73075[b]	224.87 [b]
dibenzyl ether	103-50-4	$C_{14}H_{14}O$	198.27	0.583 [g]	777.00 [b]	25.60 [b]	608.00 [b]	-	6.78621 [b]	601.40 [b]
dye (malvidin 3,5-diglucoside)	16727-30-3	$C_{29}H_{35}O_{17}Cl$	674 [d]	-	645.68 [h]	71.82 [h]	1542.50 [h]	-	4.67406 [i]	499.76 [i]

Table D.1 (continued)

Compound name	Cas Number	Formula	M_i	ω	T_c	P_c	V_c	V^*	σ_{LJ}	ε_{LJ}/k_b
			g mol^{-1}		K	bar	cm^3 mol^{-1}	cm^3 mol^{-1}	Å	K
ethanol	64-17-5	C_2H_6O	46.069	0.649 [a]	513.90 [a]	61.40 [a]	167.10 [a]	59.36 [f]	4.23738 [b]	1291.41 [b]
ethylbenzene	100-41-4	C_8H_{10}	106.17	0.302 [g]	617.20 [b]	36.00 [b]	374.00 [b]	-	5.72572 [b]	477.71 [b]
eucalyptol	470-82-6	$C_{10}H_{18}O$	154.253	0.312 [a]	695.50 [b]	31.42 [b]	509.50 [b]	-	6.18749 [i]	538.32 [i]
geraniol	106-24-1	$C_{10}H_{18}O$	300.26	0.762 [l]	739.33 [h]	15.93 [h]	820.00 [h]	-	7.61300 [i]	572.24 [i]
indole	120-72-9	C_8H_7N	117.15	0.489 [j]	790.00 [b]	43.40 [b]	431.00 [b]	-	5.84837 [b]	611.46 [b]
iodine	7553-56-2	N_2	253.809	0.107 [a]	819.00 [a]	62.79 [h]	155.00 [a]	-	5.25936 [i]	633.91 [i]
isopropanol	67-63-0	C_3H_8O	60.096	0.665 [a]	508.30 [a]	47.62 [a]	220.00 [a]	77.55 [f]	4.93749 [b]	393.42 [b]
L-carvone	6485-40-1	$C_{10}H_{14}O$	150.22	0.456 [l]	709.44 [c]	26.04 [c]	504.65 [c]	-	6.55942 [b]	549.08 [b]
linoleic acid methyl ester	112-63-0	$C_{19}H_{34}O_2$	294.47	0.465 [j]	870.78 [b]	12.54 [b]	1070.95 [b]	-	8.34769 [b]	673.98 [b]
L-menthone	14073-97-3	$C_{10}H_{18}O$	154.25	0.502 [j]	699.44 [c]	25.05 [c]	525.24 [c]	-	6.60650 [b]	541.37 [b]
methanol	67-56-1	CH_4O	32.042	0.565 [a]	512.60 [a]	80.97 [a]	118.00 [a]	41.20 [f]	3.79957 [b]	685.96 [b]
naphthalene	91-20-3	$C_{10}H_8$	128.17	0.301 [g]	748.40 [b]	40.50 [b]	413.00 [b]	-	5.85874 [b]	579.26 [b]
n-decane	124-18-5	$C_{10}H_{22}$	142.286	0.490 [a]	617.70 [a]	21.20 [a]	603.00 [a]	212.30 [f]	6.71395 [b]	434.86 [b]
n-heptane	142-82-5	C_7H_{16}	100.204	0.350 [a]	540.30 [a]	27.40 [a]	432.00 [a]	152.40 [f]	5.94356 [b]	404.05 [b]
n-hexane	110-54-3	C_6H_{14}	86.18	0.300 [a]	507.50 [a]	30.10 [a]	370.00 [a]	132.80 [f]	5.61841 [b]	434.76 [b]
n-tetradecane	629-59-4	$C_{14}H_{30}$	198.394	0.581 [a]	693.00 [a]	14.40 [a]	830.00 [a]	293.81 [m]	7.68286 [b]	536.38 [b]
octane	111-65-9	C_8H_{18}	114.23	0.399 [a]	568.80 [a]	24.90 [a]	492.00 [a]	172.30 [f]	6.17328 [b]	478.32 [b]
p-chloronitrobenzene	100-00-5	$ClC_9H_4NO_2$	157.55	0.311 [g]	817.38 [h]	43.83 [h]	390.00 [h]	-	5.87516 [i]	632.65 [i]
p-chlorotoluene	106-43-4	C_7H_7Cl	126.58	0.311 [g]	615.90 [h]	38.15 [h]	370.00 [h]	-	5.62063 [i]	476.71 [i]
perylene	198-55-0	$C_{20}H_{12}$	252.31	0.770 [l]	1030.60 [h]	25.83 [h]	770.00 [h]	-	7.31956 [i]	797.68 [i]
phenanthrene	85-01-8	C14H10	178.234	0.479 [a]	869.00 [a]	28.70 [a]	554.00 [a]	-	6.77034 [b]	675.70 [b]
pyrene	129-00-0	$C_{16}H_{10}$	202.26	0.510 [g]	936.00 [b]	26.10 [b]	630.00 [b]	-	7.11077 [b]	724.46 [b]

Table D.1 (continued)

Compound name	Cas Number	Formula	M_i	ω	T_c	P_c	V_c	V^*	σ_{LJ}	ε_{LJ}/k_b
			g mol^{-1}		K	bar	cm^3 mol^{-1}	cm^3 mol^{-1}	Å	K
tert-butylbenzene	98-06-6	$C_{10}H_{14}$	134.22	0.269 [g]	660.00 [a]	29.60 [a]	492.00 [a]	-	6.20099 [b]	510.84 [b]
tetrahydrofuran	109-99-9	C_4H_8O	72.11	0.224 [g]	540.10 [a]	51.90 [a]	224.00 [a]	70.17 [m]	4.89719 [b]	418.04 [b]
toluene	108-88-3	C_7H_8	92.141	0.263 [a]	591.80 [a]	41.0 [a]	316.00 [a]	113.90 [f]	5.45450 [b]	350.74 [b]
vitamin K3	58-27-5	$C_{11}H_8O_2$	172.18	0.619 [a]	893.85 [b]	31.96 [b]	537.20 [b]	-	6.62868 [b]	691.84 [b]

[a] Taken from Reid *et al.*[61]; [b] Taken from Magalhães *et al.*[86]; [c] Taken from Dong *et al.* [75]; [d] Taken from Mantell *et al.* [87]; [e] Calculated by the Edmister method (from [88]); [f] Taken from Kreglewski [85];[g] Average between the values estimated by the DEFINITI and LEE-KESL methods. Estimated using Aspen Plus [89]; [h] Estimated by the Joback method [86]; [i] Estimated by the Eqs.68-70; [j] Calculated by the original definition proposed by Pitzer (from Raid *et al.* [61]); [l] Calculated by the Edmister method (from [88]); [m] Taken from Aspen plus database [89].

Table D. 2 – Ternary liquid systems database, number of points of each system (NDP) and AARD obtained from the corrected TLSM-MP model.

Solute	Solvent 1	Solvent 2	NDP	AARD %
hexane	cyclohexane	benzene	3	30.91
cyclohexane	benzene	hexane	3	4.87
benzene	cyclohexane	hexane	3	11.48
acetone	cyclohexane	benzene	3	20.24
benzene	cyclohexane	acetone	3	20.39
cyclohexane	benzene	acetone	3	2.84
hexane	carbon tetrachloride	acetone	3	10.52
acetone	carbon tetrachloride	hexane	3	10.52
carbon tetrachloride	hexane	acetone	3	12.90
iodine	tetrahydrofuran	cyclohexane	3	27.08
iodine	1,4-dioxane	cyclohexane	3	13.15
iodine	benzene	ethanol	4	33.95
iodine	toluene	ethanol	3	31.94
iodine	carbon tetrachloride	ethanol	3	22.79
iodine	n-hexane	ethanol	4	7.49
iodine	cyclohexane	ethanol	4	26.19
toluene	n-tetradecane	n-hexane	6	24.83
toluene	cyclohexane	n-hexane	3	19.79
toluene	n-hexane	cyclohexane	3	3.130
benzene	n-heptane	n-hexane	9	2.030
chlorobenzene	n-heptane	n-hexane	9	0.30
ethylbenzene	n-heptane	n-hexane	9	4.23
toluene	n-heptane	n-hexane	9	0.89
p-chlorotoluene	n-heptane	n-hexane	9	6.16
naphthalene	n-heptane	n-hexane	9	5.72
pyrene	n-heptane	n-hexane	9	6.65
perylene	n-heptane	n-hexane	9	3.03
benzene	ethanol	n-hexane	8	7.70
benzene	ethanol	acetone	8	23.43
benzene	octane	n-hexane	9	1.84
chlorobenzene	octane	n-hexane	9	8.74
ethylbenzene	octane	n-hexane	9	7.85
toluene	octane	n-hexane	9	9.78
p-chlorotoluene	octane	n-hexane	9	6.14
naphthalene	octane	n-hexane	9	5.87
pyrene	octane	n-hexane	9	6.43
perylene	octane	n-hexane	9	8.71
benzene	n-decane	n-hexane	5	10.72

Table D.2 (continued)

Solute	Solvent 1	Solvent 2	NDP	AARD %
chlorobenzene	n-decane	n-hexane	5	11.87
ethylbenzene	n-decane	n-hexane	5	8.78
toluene	n-decane	n-hexane	5	12.75
p-chlorotoluene	n-decane	n-hexane	5	5.93
naphthalene	n-decane	n-hexane	5	5.92
pyrene	n-decane	n-hexane	5	7.29
perylene	n-decane	n-hexane	5	11.02
benzene	n-octane	n-heptane	9	3.58
chlorobenzene	n-octane	n-heptane	9	3.11
ethylbenzene	n-octane	n-heptane	9	16.60
toluene	n-octane	n-heptane	9	21.01
p-chlorotoluene	n-octane	n-heptane	9	13.57
naphthalene	n-octane	n-heptane	9	15.54
pyrene	n-octane	n-heptane	9	14.37
benzene	n-octane	n-decane	8	15.35
chlorobenzene	n-octane	n-decane	8	17.43
ethylbenzene	n-octane	n-decane	8	16.81
toluene	n-octane	n-decane	8	17.59
p-chlorotoluene	n-octane	n-decane	8	17.53
naphthalene	n-octane	n-decane	8	16.69
pyrene	n-octane	n-decane	8	17.03
perylene	n-octane	n-decane	8	16.88
benzene	n-hexane	cyclohexane	7	11.08
chlorobenzene	n-hexane	cyclohexane	7	4.61
ethylbenzene	n-hexane	cyclohexane	7	2.26
toluene	n-hexane	cyclohexane	7	6.93
p-chlorotoluene	n-hexane	cyclohexane	7	1.35
naphthalene	n-hexane	cyclohexane	7	4.24
pyrene	n-hexane	cyclohexane	7	5.41
perylene	n-hexane	cyclohexane	7	3.52
benzene	n-heptane	cyclohexane	7	8.10
chlorobenzene	n-heptane	cyclohexane	7	5.24
ethylbenzene	n-heptane	cyclohexane	7	4.06
toluene	n-heptane	cyclohexane	7	5.55
p-chlorotoluene	n-heptane	cyclohexane	7	3.63
naphthalene	n-heptane	cyclohexane	7	1.52
pyrene	n-heptane	cyclohexane	7	3.76
perylene	n-heptane	cyclohexane	7	3.80
benzene	n-octane	cyclohexane	6	7.72

Table D.2 (continued)

Solute	Solvent 1	Solvent 2	NDP	AARD %
chlorobenzene	n-octane	cyclohexane	6	7.08
ethylbenzene	n-octane	cyclohexane	6	1.85
toluene	n-octane	cyclohexane	6	3.71
p-chlorotoluene	n-octane	cyclohexane	6	1.17
naphthalene	n-octane	cyclohexane	6	3.12
pyrene	n-octane	cyclohexane	6	1.50
perylene	n-octane	cyclohexane	6	6.85
benzene	n-decane	cyclohexane	5	5.26
chlorobenzene	n-decane	cyclohexane	5	16.53
ethylbenzene	n-decane	cyclohexane	5	7.68
toluene	n-decane	cyclohexane	5	6.85
p-chlorotoluene	n-decane	cyclohexane	5	7.97
naphthalene	n-decane	cyclohexane	5	11.15
pyrene	n-decane	cyclohexane	5	9.33
perylene	n-decane	cyclohexane	5	18.38

Table D. 3 – Ternary SCF systems database, number of points of each system (NDP) and AARD obtained from the corrected TLSM-MP model.

Solute	Solvent 1	Solvent 2	NDP	AARD %
benzoic acid	carbon dioxide	methanol	9	23.16
phenanthrene	carbon dioxide	methanol	9	15.19
acridine	carbon dioxide	methanol	9	6.10
linoleic acid methyl ester	carbon dioxide	n-hexane	13	20.98
vitamin K3	carbon dioxide	n-hexane	29	8.63
indole	carbon dioxide	n-hexane	13	6.65
benzyl acetate	carbon dioxide	ethanol	90	2.88
2-phenylethyl acetate	carbon dioxide	ethanol	90	2.37
3-phenylpropyl acetate	carbon dioxide	ethanol	90	2.84
dibenzyl ether	carbon dioxide	ethanol	90	3.97
vitamin K3	methanol	carbon dioxide	53	12.20
L-carvone	carbon dioxide	ethanol	46	7.10
L-menthone	carbon dioxide	ethanol	46	4.79
2-nitroanisole	carbon dioxide	methanol	30	5.06
2-nitroanisole	carbon dioxide	n-hexane	15	17.55
1,2-dichlorobenzene	carbon dioxide	methanol	30	6.85
1,2-dichlorobenzene	carbon dioxide	n-hexane	15	20.65
tert-butylbenzene	carbon dioxide	methanol	30	4.08
tert-butylbenzene	carbon dioxide	n-hexane	15	9.57

Table D.3 (continued)

Solute	Solvent 1	Solvent 2	NDP	AARD %
3-fluorophenol	carbon dioxide	n-hexane	6	3.96
3-fluorophenol	carbon dioxide	tetrahydrofuran	6	29.37
3-fluorophenol	carbon dioxide	methanol	6	40.66
3-fluorophenol	carbon dioxide	acetonitrile	4	22.89
3-fluorophenol	carbon dioxide	isopropanol	6	33.87
1,3-dichlorobenzene	carbon dioxide	n-hexane	6	9.04
1,3-dichlorobenzene	carbon dioxide	tetrahydrofuran	6	4.13
1,3-dichlorobenzene	carbon dioxide	methanol	6	3.64
1,3-dichlorobenzene	carbon dioxide	acetonitrile	4	2.98
1,3-dichlorobenzene	carbon dioxide	isopropanol	6	14.95
L-carvone	carbon dioxide	n-hexane	6	2.39
L-carvone	carbon dioxide	tetrahydrofuran	6	5.57
L-carvone	carbon dioxide	methanol	6	7.93
L-carvone	carbon dioxide	acetonitrile	4	2.77
L-carvone	carbon dioxide	isopropanol	6	6.50
geraniol	carbon dioxide	n-hexane	6	6.02
geraniol	carbon dioxide	tetrahydrofuran	6	6.03
geraniol	carbon dioxide	methanol	6	13.01
geraniol	carbon dioxide	acetonitrile	4	4.54
geraniol	carbon dioxide	isopropanol	6	9.15
gallic acid	carbon dioxide	ethanol	9	24.36
eucalyptol	carbon dioxide	ethanol	24	11.41